2015

Damage detection through acoustic emission of fracture processes in concrete masonry units

John Alexander Cain

DAMAGE DETECTION THROUGH ACOUSTIC EMISSION OF FRACTURE PROCESSES IN CONCRETE MASONRY UNITS

by

JOHN ALEXANDER CAIN

A THESIS

Presented to the Faculty of the Graduate School of the

MISSOURI UNIVERSITY OF SCIENCE AND TECHNOLOGY

In Partial Fulfillment of the Requirements for the Degree

MASTER OF SCIENCE IN CIVIL ENGINEERING

2015

Approved by

Dr. Genda Chen, Advisor
Dr. Mohamed Elgawady
Dr. Lesley Sneed
Dr. Daniel Stutts

ABSTRACT

Masonry structures are vulnerable to earthquakes; their brittleness and discontinuous formation make them susceptible to collapse. In the event of an emergency, this could be detrimental and perhaps fatal. The area of Structural Health Monitoring (SHM) is focused on understanding the behavior of structures for the sake of safety and predicting their longevity. One applicable technique to monitor this behavior is Acoustic Emission (AE). Acoustic Emissions are transient elastic waves released as microcracks nucleate from stress intensities, coalesce into cracks and then accumulate as damage. AE monitoring is a favorable method because it is capable of detecting cracking from within a given solid while in operation and over a long time span.

Having a clear understanding of the fracture process can help engineers find the underlining problems with an existing structure, which is vital information for rehabilitation and guarded usage. In this study, AE signals (Hits) were collected from cyclic compression tests of experimental Concrete Masonry Units (CMU) prisms and cyclic lateral tests of experimental post-tensioned CMU shear walls. The tests captured the damage process of CMU as it was brought to failure. Quantitative parameters of the recorded AE hits were studied and a greater understanding of the underlining AE behavior of fracture within masonry was achieved.

ACKNOWLEDGMENTS

I would like to thank a number of people who helped make the completion of this work possible, most especially my advisor, Dr. Genda Chen, for his experience and generosity in funding this experimental work, Dr. ElGawady and Ahmed Gheni for leading the research in masonry and Dr. Sneed and Dr. Stutts who were encouraging and knowledgeable in and out of the classroom. I also would like to thank John, Georgia, Demetria and Pouli for their love and support during all of the hard times and fun times of life. I would also like to thank my friends for helping me get through the hard times and fun times of graduate school. Lastly, I would like to thank the community at Missouri S&T for meeting and exceeding my expectations.

TABLE OF CONTENTS

Page

LIST OF ILLUSTRATIONS

Figure Page

LIST OF TABLES

Table Page

1. INTRODUCTION

Masonry structures are highly susceptible to failure from lateral movements caused by earthquakes. In high seismic areas such as California, tough standards have been implemented to safe guard the public against vulnerable masonry buildings. Having a method to determine the integrity of a brick building which has been subjected to severe earthquakes can help engineers determine risks to occupants. Acoustic Emission (AE) sensing technology is a suitable method for monitoring structures while in operation. Though AE is a passive form of nondestructive testing (NDT), meaning it can only capture damage as it is occurring, it has the benefit of continuous real-time monitoring. This information can provide a description of damage incurred as a result. It is also especially useful in monitoring internal defects or parts of structures that are impossible or impractical to access.

Concrete Masonry Units (CMU) are of interest because of their ubiquity as a construction material. Currently, there is little research in the area of monitoring masonry structures with AE. With more proven studies showing the reliability of this information, it may be possible to implement this technology. Critically in this discussion, the AE sensor is only effective when it can sense sounds that are not attenuated. Beyond the sensing radius, even strong signals are unobtainable. Given the other available options for sensing cracks, AE has the benefit of sensing cracks within a brick, without affecting structural integrity and over a fairly significant area.

In this document, two different studies were done using the same sensing technology to understand the process of damage. This approach took into account the effect of specimen size to help capture the local and global effects to CMU as it underwent damage. One study was a small setup, which involved masonry prisms loaded cyclically in uniaxial compression. The second was a full-scale wall system tested under earthquake loads. These studies were displacement controlled cyclic tests that looked at the effect of repetitive loading until failure. This research is part of another project pursued by Dr.

Mohamed Elgawady and his graduate student, Ahemd Gheni, at Missouri S&T. Their goal is improving the structural performance of masonry.

In these tests, two different types of sensors were used: a low frequency resonating sensor and a higher frequency wideband sensor. The use of the two sensors gives the perspective of helping to capture spectral changes as the damage progressed from microcracking to macrocracking, and the overall effect of sound propagation in a material. Hardware settings of the technology were defined to capture as much reliable data without the influence of noise. Different sensor configurations were tried and threshold levels were adjusted to take into account forecasted damage. In real life applications, environmental noise can greatly impact the results. Having a method of accounting for this is crucial.

Results of AE parameters such as hits, amplitude, counts, frequency centroid, and signal strength are correlated directly with the benchmark of either force or displacement from actuators. The load value is often displayed as another data set within each plot and is clearly labeled. The results are shown temporally and in many cases have been cumulated to represent quantitatively the overall changes to the wave parameters throughout each test. Sensor results were also grouped in this study based on type and location to efficiently express this large data set. This analysis focused on Hits because Event analysis lacked reliability. Averaged values of some of these parameters were also studied because of the effects of scatter in each data set. Since there is very little literature on monitoring CMU under earthquake loading, this research may be a first attempt at grasping the underlining AE behavior of large CMU structures brought to failure.

2. LITERATURE REVIEW

2.1. RESEARCH SIGNIFICANCE

The necessity of studying distressed structures has provoked scientists and engineers to pursue paths toward evaluation and characterization of limit states of essential facilities and infrastructure. Given its benefits as an evaluation method, Acoustic Emission (AE) is a powerful tool in the arsenal of monitoring techniques. This technology can be applied to observing in real-time continuous mechanisms of structures while in use. This information is beneficial for researchers and engineers of record to forecast a timeline of operation or devise a rehabilitation plan. In conjunction with other available technologies, the information gathered from AE could be vital for making a decision that would affect the safety of the public.

The focus of AE research in Civil Engineering in recent years has been mostly related to advances in the capabilities of the technology to observe damage to concrete structures. Concrete is the most widely used building material because of its versatility and relatively low cost. The subject of this study is the Concrete Masonry Unit, which is used as a common element in buildings.

Just like any other commonly used material, CMU are not indestructible and so are susceptible to a variety of different failure mechanisms such as overstressing, fatigue, fracture, spalling, and corrosion-induced cracking. To fulfill their functions properly, repair and rehabilitation of the structures may be required. For this purpose, it is necessary to have a full understanding of the state of deterioration. The assessment of the damage or the structural integrity in the existing concrete structures is neither an easy task nor a practically standardized procedure.

AE technology has been successfully used in both laboratory and field settings. The ability for AE systems to detect cracking within a structure makes it an interesting method to determine the stabilization or progression of damage. AE is an extremely

sensitive method of registering cracking within a structure. Though not completely confirmed in the literature, it was pointed out that AE could detect internal cracks in concrete around 1mm (0.04) or less within a structure (Ohtsu, 1989). With all of the possibilities of this technology, the primary goal of AE monitoring in structures is to detect, locate, and assess the intensity of damage (Holford and Lark, 2005).

2.2. BASICS OF NON-DESTRUCTIVE TESTING

There is significant motivation to accurately determine the state of an aged or damaged structure. Non-destructive testing (NDT) is the field of testing which incorporates a variety of techniques to evaluate properties of a material, component or system without causing damage. Other names for NDT include nondestructive examination (NDE), nondestructive inspection (NDI) or nondestructive evaluation (NDE). These all essentially refer to the same approach. The most readily available and effective form of NDT for engineered structures is visual inspection. Like other methods, this basic type of evaluation requires the observer to possess a basic understanding of engineering.

Of the developed techniques of observation, there are several examples of NDT: ultrasonic, magnetic-particle, liquid penetrant, radiographic, remote visual inspection, eddy-current testing, and low coherence interferometry (Losert, 2009). NDT is principally used in engineering applications, but also applied in medicine and art (Cartz, 1995). Structural Health Monitoring (SHM) is related to the practice of different usages of NDT methods or combining these to evaluate the condition of existing structures.

SHM processes involve the observation of a system over time using periodically sampled response measurements from an array of sensors, the extraction of damage-sensitive features from these measurements and statistical analysis to determine the actual state of an existing structure. After an extreme event, such as an earthquake or explosion, SHM can be used for rapid condition screening and aims to provide, in near real time, reliable information regarding the integrity of the structure (Dawson, 1976). SHM provides important information for maintaining structures within safe levels

of operation. Such monitoring consists of estimating damage severity. This information is relevant for estimation of the vulnerability of a structure to future earthquakes and also provides useful information for optimization of maintenance costs (Castellanos and Ordaz, 2014).

General guidelines for SHM using AE is prescribed by the American Society of Testing and Materials in the standard, ASTM E2983-14. This standard indicates five unique stages for successful implementation.

2.2.1. AE-SHM Procedure Development. Diagnosis distinguishes typical noise-related AE from material-generated noise from cracking. The diagnosis is performed based on collected data, numerical modeling, background history, and a NDE database.

2.2.2. Sensing. Sensing captures data and measurement of the subject with additional parametric information such as force, pressure, temperature, and strain following a SHM procedure.

2.2.3. Diagnosis. Diagnosis distinguishes typical noise-related AE from material-generated noise from cracking. The diagnosis is performed based on collected data, numerical modeling, background history, and a NDE database.

2.2.4. Monitoring. Data are continuously collected from periodic or continuous sampling, observing conditions when the testing occurred.

2.2.5. Prediction. A prediction is defined by an appropriate reinspection or monitoring policy based on diagnostic and monitoring results. It is an assessment of suitability for continued service of the structure from a factual understanding of the structure behavior based statistical or numerical means.

NDE and diagnostics techniques for concrete structures have recently become in great demand for maintenance purposes. All over the world, the repair and retrofitting of aged concrete structures is becoming more common because of the cost savings over complete reconstruction (Ohtsu and Watanabe, 2001). With the given demand of repair

and bridge maintenance, a foolproof reliable method of evaluation would be useful. The advances in testing are a great asset which can actually save money.

Having an automated approach can allow for long observation that brings about more reliable results. Compared to visual inspection, AE is a powerful tool to quantifying damage within a structure.

2.3. BASICS OF ACOUSTIC EMISSION IN CIVIL ENGINEERING

The basis of this research has been to use AE sensing to examine a variety of different limit states with structures made of cementitious materials that are quasi-brittle, potentially leading to rapid failure of the component in question. AE are transient elastic waves within a material and are caused by the release of localized stress energy (Hu, Lu et al., 2013). The wave is a combination of longitudinal, shear and Rayleigh waves.

The AE sensor is sensitive to these elastic waves that travel through the structure. The sounds which are collected are usually in a spectrum above the range of human hearing. The response of these sensors can be classified into two groups: burst signals and continuous waves. A burst signal is shown in Figure 2.1a and is characterized by one dominant peak and smaller amplitude peaks with concentrated energy within a short time, which is a random vibration for the entire duration of the recorded signal length, hence no definitive pattern.

2.4. BRIEF HISTORY OF AE TECHNOLOGY APPLICATIONS

The earliest published studies of experimentation with AE occurred in the early 1940s in the area of rock mechanics, which are still used to predict rock bursts in mines. The first application of this technology to metals was carried out by J. Kaiser, who conducted tests with steel, zinc, aluminum, copper and lead in the 1950s. From these tests, he discovered an absence of acoustic emission in materials under stress levels below those previously applied. This effect, bearing the name of Kaiser, is still widely used.

Research done in recent decades has revealed that the Kaiser effect is a material specific property and not all materials exhibit this behavior.

LHermite measured acoustic emission from concrete, finding a sharp increase in acoustic waves coinciding with significant matrix cracking. In the 1960s in parallel efforts, the USA and the Soviet Union used acoustic emission for assessment of structural integrity of rocket motor cases. In the Soviet Union, AE was also used in the prediction of coal burst and fracture of rocks (Shamina, 1956; Vinogradov, 1964; Knill et al. 1968). One major advancement in this field occurred in 1965 when Robinson used more sensitive equipment to monitor microcracking within materials. H. Dunegan proposed the use of AE for inspection of pressure vessels and in 1969 founded the first AE Company in the USA. Since then, research institutes have developed application for crack detection, material studies and non-destructive control of various structures (mostly military-related). In 1970, a more sensitive apparatus was built by Wells to monitor acoustic emissions in the range of 2 kHz to 20 kHz. Green reported a much more extensive series of test, recording acoustic emission frequencies up to 100 kHz which lead to the process of source location techniques. From the tests, he was able to detect locations of defects. With technologies at the time, Green also discovered that the Kaiser effect, in essence, did not apply to concretes as was once believed.

The earliest recorded practical use of AE was to monitor portable military bridges subjected to proof testing in the 1970s by Pollock and Smith, who studied a portable tank bridge for the British Ministry of Defense. They were able to correlate information from testing in the laboratory with field results (Parmar and Sharp 2009). In 1972, the Argronne National Laboratory proposed to monitor AE from a bridge on I-80 in Illinois. An extensive program funded by the Federal Highway Administration (FHWA) with Battelle Pacific Northwest in the late 1970s resulted in the development of a battery powered digital acoustic emission monitoring system (Hutton and Skorpik, 1977). In the 1980s, long-term continuous monitoring implemented on a bridge was conducted by the Dunegan Corporation. In these tests, it was determined that months of filtering would

be necessary for eliminated environmental noise. Miller et al. assessed both time and frequency of the signals to distinguish various sources. Guidelines meant for local and global monitoring of steel bridges were developed by a number of researchers, including Pollock and Carlyle, Carter and Holford, and Pullin et al.

Research has been conducted to monitor corrosion of reinforcement, and its resulting damage, including spalling and crack extension. Corrosion study is another area of research. Work by Yuyama and Ohstu studied the fracture characteristic, quantifying microfractures and damage intensity in concrete. The effect of attenuation was the subject of Lands, Shah and Beck who investigated acoustic emission in bridges. Between 1996-2000, the NDE validation Center in Virginia conducted AE testing to monitor cracking as a result of overloaded bridges.

Researchers in Poland have conducted similar experiments on concrete bridges, by overloading them and collecting the acoustic emissions by the cracked members. Monitoring of prestressed concrete bridges was also reported by Vogel et al. There has been interest in the monitoring of prestress or post-stress concrete structures. A company called Pure Technologies has developed a SoundPrint which locates wire breaks in prestressing tendons (Paulson, Elliott et al., 2001).

For future work in engineering, engineered cementitious composites have shown to provide better resistance to cracking and thus higher toughness. Though not conventionally used in engineered structures, their applications have good benefits. Research has been conducted by Ziehl and Bane to monitor fiber reinforced polymers with AE during cyclic loading. In these studies, AE was quite useful in registering cracking before it would become an issue with bridge decks. AE has also been used in new structural composites to evaluate damage.

Advances in technology have greatly improved sensors by making them more compact, sensitive and economically viable. Interest in the field has lead toward creating networks of wireless sensors that can continuously collect data. Remote sensing is a desirable feature of sensing technology for its abilities to be a permanent fixture on a bridge system.

Having a longer sample history can greatly improve the analysis for a structure and thus provide more conclusive results about the structures behavior. In the past, the Local Area Monitoring (LAM) is one such AE monitoring instrument developed by Physical Acoustics Corporation (PAC) in collaboration with the Federal Highway Administration, and has proposed developing a monitoring system that identifies rebar corrosion. In the future, with a highly evolved base of knowledge, more technology could be developed and implemented to remotely monitor structures .

AE has been of interest to researchers in concrete technologies for over 40 years, with the goal of eventually incorporating the technology into civil structures. With this goal in mind, there are many practical hurdles that still need to be conquered. Ohtsu's technique for sound location and moment tensor analysis utilized a large sensor array to study a small volume. Often times a multiple sensor array would not be practical for real world applications because of the requirement of multiple sensors and access to all sides of a structure.

Quantitative treatment of AE results are being applied to practical use. In Japan, there is a high demand due to the prevailing and cumulative effect of earthquakes on existing structures (Ohtsu, Uchida et al. 2002). According to the Japanese Society for Non-Destructive Inspection, the recommended practice for in-place monitoring of concrete structures by AE is currently established.

More recently, research has been done using sensors sparingly and applying statistical techniques to infer damage. In this area of concrete technology, Farhidzadeh, Mpalaska and Matikas have developed a method for crack identification with statistical analysis that could be more beneficial because it would be possible to cover a large volume with fewer sensors (Farhidzadeh, Mpalaskas et al., 2014). Due to the market price of one of these systems, this approach is the most realistic.

2.5. CORRELATION BETWEEN CRACKING AND LOAD DATA

Many researchers have studied AE and notched concrete beams, measuring crack opening based on crack mouth open displacement. Based on the study Evaluation of Concrete Fracture Procedure Based on Acoustic Emission Parameters, it was found that the characteristics of AE parameters could reflect the concrete crack propagation and its complete structural failure during the loading procedure. It was found that the results from AE method were similar to those from strain gauge methods, by investigating the results on concrete notched beam specimens of two different sizes. In this study, a damage ratio was used as a measurement of damage:

$$DamageRatio = \frac{N}{N_s} \tag{2.1}$$

where N is the current amount of accumulated Hits and N_s is the total amount of Hits. This particular method, strictly limited to hit quantities, is a type of indicator of damage and is convenient enough to be used for bending tests of notched beams. In their study, small crack lengths resulted in very low damage ratios regardless of the beams height. In terms of stress and damage ratio, at stress levels below 80% of total tensile strength, the damage ratios were rather insignificant. Their results also proved that higher crack length to beam height resulted in a greater damage ratio regardless of beam size (Hu, Lu et al. 2013). In all of these tests, at high deflection there was an obvious decrease in load resistance after rapid crack growth as a result of energy release by the structure. The cracking stabilized with the decrease in load until eventual failure of the entire member. Showing that sounds are produced by crack propagation and at stable crack growth, few signals were created, which corresponds with less energy dissipation.

2.6. AE PARAMETERS

The burst signal seen in Figure 2.1a may represent many interesting phenomena. It is the response of a lead zironate titanate (PZT) element, so the properties of the

sensor greatly matter. The parameters of the wave are determined by the software and are shown in this figure. Quantifying and then analyzing the results is the approach to understanding the random phenomena of sound generation from cracking. The output of the sensor can have the scale of either mV or dB which are related by equation 2.2

$$dB = 20log_{10}(\frac{V}{10^{-6}}) - (Preamplifier\ Gain\ in\ dB) \tag{2.2}$$

where V is the recorded wave amplitude in volts. Figure 2.1b shows a continuous signal which is representative of significant AE activity. From the research conducted in this study, these signals were encountered at moments of significant cracking such as at the peak of a new load step.

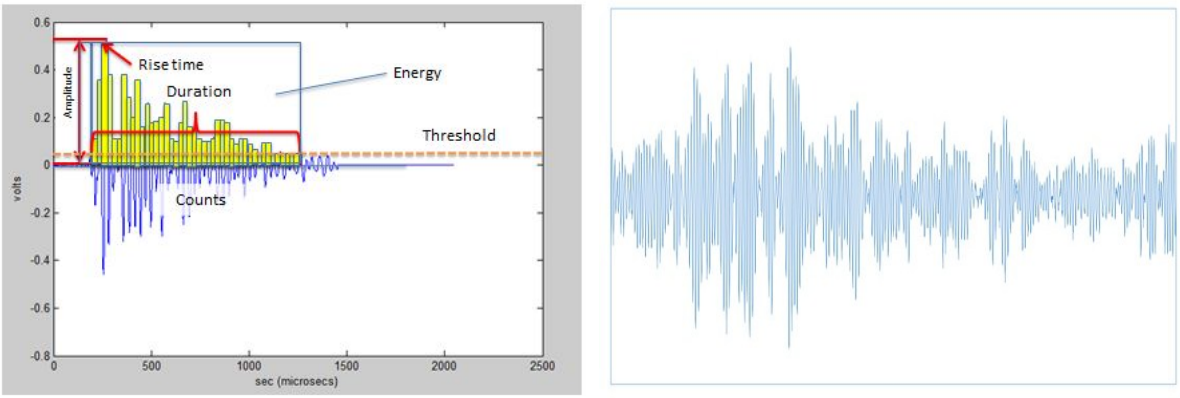

(a) Burst signal with AE parameters (b) Continuous waveform

Figure 2.1. Recorded acoustic emission Hits

2.7. AE SYSTEM STRUCTURE

The AE system requires an array of sensors that are connected to a hardware device which convert the signals into a format that a computer can store and analyze. The system used in this research was developed by the Mistras Group a subsidiary of the Physical Acoustics Corporation. The sensor is coupled or mounted to the surface of the subject. A coupling method used could be an adhesive or a grease. The objective is to

create a perfect contact between the surface of the sensor and the surface of the material so that good frequency response can be represented.

The sensor will produce a voltage as a result of the response or vibration of a PZT ceramic. That signal will be transmitted with the coaxial cable to the hardware component either built in the computer or external. The system used a peripheral component interconnect (PCI) card with 8 input channels. The PCI card has a gain amplifier, filters, buffer and an analog-to-digital converter built into it. This particular card has 4-high-pass and 4-low-pass filters and a 16 bit A/D converter module where the AE signal is digitized at rates up to 3.0 MHz and can transfer 132 Mbytes/sec to a computer. Each card also has LED drivers that light up on the front of the CPU casing, showing the activity of each channel.

There are two different types of software which are presented by Mistras: AEwin and Noesis. AEwin is a software designed for collecting the signals, and Noesis is designed for post-processing. The AEwin runs while the testing is performed. While using AEwin, the user will need to adjust the hardware settings so that the desired signals are recorded with the desired content. Without some calibration, it is very easy for the machine to miss many of the qualities of each recorded wave or to record noise. Within AEwin, the user has the ability to setup location analysis. For some materials, this location approach can be quite beneficial in determining where cracking has occurred. Due to the heterogeneity, precise location of cracking in concrete proves to be quite challenging. Information on this approach is presented in Section 2.12. AEwin has built-in functions to perform the analysis of the waves. Through graphing capabilities, the user can see in real-time the results of the test while signals are being recorded. When tests are performed, almost all of the hardware settings such as bandwidth, sampling rate, and pre-trigger are locked along with software settings like Peak Definition Time, Hit Definition Time and Hit Lockout Time. Graphing results are presented in AEwin in real-time, and the user has the ability to determine if settings need to be adjusted. The test will be recorded in DTA format that can be replayed in AEwin or Noesis with different graphical

configurations. Filters can also be activated. In presenting information graphically, the software is designed to average parameter values based on a bin size. This will have an effect on the amount of data points.

Noesis can provide more analysis techniques and output functions that, for much of wave parameters, is based on a single wave instead of using bins. One of the main limitations with AEwin is that the user does not have the option to study individual waves. Each individual wave can be studied in Noesis. Features, such as Peak Amplitude, Counts and Frequency Centroid can be studied within the softwares environment or outputted as raw data. Some of the results presented were created using an average approach, such as the average frequency centroid. This can be considered a limitation, because the rate at which signals are stored with averaged signal parameters, some of the behavior can be misrepresented. The greatest benefit of Noesis is its power to perform supervised and unsupervised clustering of signals and training data. By clustering recorded sounds, those identified clusters can be applied to other data sets to identify particular types of sounds that are repeated from test to test.

2.8. SOUND PROPAGATION IN MEDIA

Sounds that travel through structures are transient elastic waves produced by physical Events within the material. As previously stated, these waves include primary waves (longitudinal), secondary waves (shear), and Rayleigh waves which travel across the surface of the structure. All of these waves are present when sound or noises are transmitted through concrete. The presence of this variety of waves is the mechanism that causes the response of the AE transducer, thus producing an electrical signal which is then recorded by the PCI hardware. The study of the physical properties of sound is important in interpreting data from the test and thus understanding the behavior of the structure.

The goal of this and other NDT methods is to evaluate a structure's performance. Damage will be due to stresses or forces that are dispersed across a theoretical plane with

material or chemical changes to the material as a result of environmental effects. Forces are generally categorized as tensile, compressive, bending, shear or torsional. To really understand the system, it is important to consider what happens on the atomic level as forces are being transmitted between bodies. Stress causes atoms to move away or closer to each other, resulting in a physical change in the shape of a body. This transcending change causes noticeable effects on the micro and macroscopic level. The material will deform elastically. When that change is dramatic enough, the material's atomic bonds will reorganize and this irreversible process will cause permanent deformation. This deformation will be coupled with a release of energy in the form of elastic waves which flow in every direction within the structure. In general, it should be noted that the damage to metals such as steel will be due to dislocations as well as fractures with new surface creation. For brittle and quasi-brittle materials like concrete, plastic deformations will be due to the formation of cracks or crushing of the matrix. The study of fracture mechanics addresses the phenomenon of atomic bond breaking in an in-depth level that supports the theoretical methods to assess given systems subjected to a variety of different stress states. Information on this topic will need to be addressed further in this discussion.

The properties of the material have a great impact on the elastic waves as they flow through the structure. In certain studies which evaluate the time of arrival (TOA) of signals, there can be major differences in the arrival time of AE signals in concrete. This makes the use of single wave velocity as required in the TOA method very difficult due to the variety of wave velocities obtained, especially for large structures (Muhamad Bunnori, Pullin et al., 2006). Homogenous materials, such as steel, have well-defined velocities, but concrete being a composite of sand, rock, cement, air and steel rebar proves to be quite heterogeneous and thus less predictable and harder to quantify (Muhamad Bunnori, Pullin et al., 2006). In general, several key assumptions can be made about sound in concrete and material properties. Propagation of sounds in concrete can be quite different due to the age of the concrete, the water to cement ratio, the aggregate to cement content, the concrete strength, concrete cover thickness and steel bar spacing.

Also important is the shape of the specimen being tested and the length in which sounds travel from source to sensor (Muhamad Bunnori, Pullin et al., 2006). Muhamad Bunnori, Pullin and et al found in their study of concrete specimens that the waves within the beams had a faster wave velocity than slabs.

In many cases, the waves that reach each of the sensors are a combination of several types of basic modes. The waves that are received by the sensor from a source may be the result of several different types of modes combined to create a unique signal.

The time of arrival (TOA) method for source location has been implemented to determine locations of signals within a structure. As discussed earlier, cementitious materials present many challenges in accurately representing locations of signals from the data collected from multiple sensors. Many complications can arise when using the method of TOA for larger structures due to the conversions of modes, dispersion and attenuation of waves. (Prosser, Hamstad et al., 1999). In contrast, in a homogeneous structural member such as thin metal sheets, early low-amplitude (weak) fast arriving reached the sensor first, followed by a threshold passing wave and a high-energy late arriving waves' which consists of extensional and shear waves (Kaphle, Tan et al. 2012).

The concept of attenuation plays a significant role in the signal quality. The effect of attenuation for sensors is not only a loss of signal strength but also signal characteristics. For many materials, the distance of just a couple of feet can have a large impact on the recorded signal strength. For concrete, the signals lose 50% of amplitude for every double in distance between sensors. Lower frequency sounds or larger wavelengths travel further and are less susceptible to discontinuities within the material. Knowing that frequencies are inversely proportional to wavelength, the higher frequency component of the waves signal will be attenuated before other parts of the signal.

For concretes and their heterogeneous structure, the sounds will be altered as the waves pass through the variety of medium with varying elastic modules such as Portland cement, sand and gravel. In many cases, the actual shape of the structure plays an important role in how the reflections of the sound interact when the wave is captured. In

tests which involve long narrow specimens such as rods, the intensity of the signal will be preserved and thus it will be less affected by attenuation (Muhamad Bunnori, Pullin et al. 2006). For studies related to concrete, this observation is almost never the case; therefore, attenuation needs to be taken into account in planning a sensory array. In this study, cracking played an important role in the results recorded by each sensor. From the results discussed it was found that cracking causes attenuation due to the increase in the number of interfaces of crack surfaces and voids.

Absorption of the sound's intensity will be caused by differences in the material modulus as well as the presence of discontinuities which prevent the signal from passing as a complete wave. The elastic and kinetic energies in the wave are absorbed and converted into heat by internal friction. There should be an account for loss of energy as the wave fronts move further away from the source.

The level of stress is also important on the behavior of sound. With an increase in stress, the velocity of surface wave propagation is increased from closing of microcracks within the material. Similarly, the average frequencies of signals also tends to increase due to the reduced attenuation. (Shokouhi, Zoga et al. 2012) With stress that is sufficient enough to cause damage, the velocity of waves will decrease as new microcracks begin to form and the path of sound waves is hindered by these small openings (Shokouhi, Zoga et al. 2012).

2.9. TYPES OF SENSORS

The sensor consists of a strong durable casing with a wearing plate coupled to the material surface. Vibration to the PZT ceramic as. The process is known as a direct piezoelectric effect referring to the charge produced when a piezoelectric substance is subjected to a stress or strain producing an electrical charge. This charge will travel some distance through coaxial cable until it reaches the PCI. The PCI will do all of the necessary processing and store the waves as DTA file. Sensors can be divided into three categories: resonant, wide bandwidth, and R-type. These types are shown in Figure 2.2.

The understanding of the qualities of the sensor is necessary to determine which type of instrument is suitable for the application and what can be understood by their electrical signal. For applications where the source frequency is known, a resonant sensor (see Figure 2.2a) can be fitted to that frequency. For applications where a variety of different signal frequencies are observed from a source, a wideband sensor (see Figure 2.2b) can be selected so that it is capable of detecting several different types of signals. The R type sensor (see Figure 2.2c) which has a preamplifier built in is capable of amplifying the output signal from the PZT. The R-Type sensor has the advantage of high signal to noise ratio by reducing the effect of impedance.

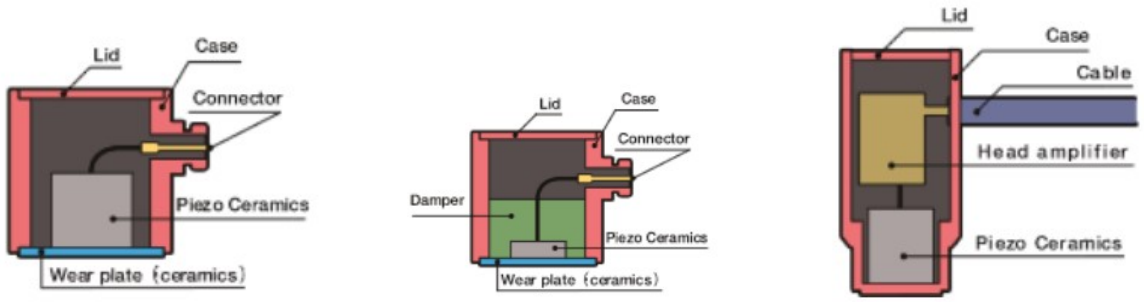

(a) Resonant Sensor (b) Wideband Sensor (c) R-Type Sensor

Figure 2.2. Types of sensors (Fuji Ceramics Corporation)

These types of sensors also have the ability to test calibration by functioning as an actuator in which case, the sensor will send elastic waves through the material, simulating a source.

Two types of sensors (R1.5 AST and F15i AST) both have a built-in preamplifier which is desirable for sending signals through longer distances of cable. The AST (Auto Sensor Test) feature of these sensors makes it capable of sending mechanical pulses. This is advantageous for calibrations when the user doesnt have access to the location. As shown in Figure 2.2c and with a response shown in Figure 2.3, the R1.5 AST sensor has a resonant frequency of 14 kHz which is capable of detecting low frequencies. As would be expected, these low frequencies are less susceptible to attenuation than higher frequencies and can be detected at further distances. The F15I sensor shown in Figure 2.4 is a wide

bandwidth sensor and has a flat response and is capable of detecting signals in a higher frequency. It is designed as a wideband sensor for that ability to have a similar response over a designated spectrum. The sensor has the same AST feature.

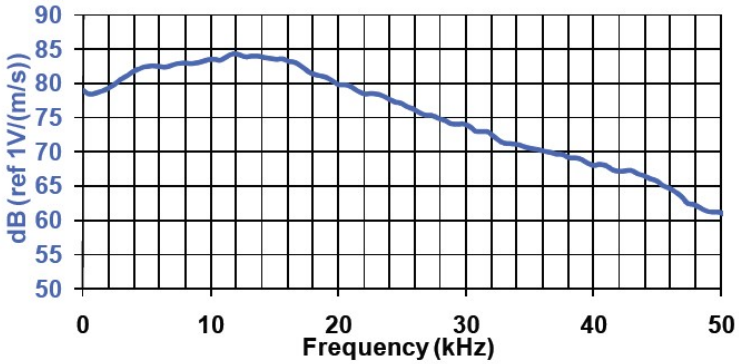

Figure 2.3. R1.5 AST resonator sensor response with 14 kHz peak resonant frequency shown in kHz

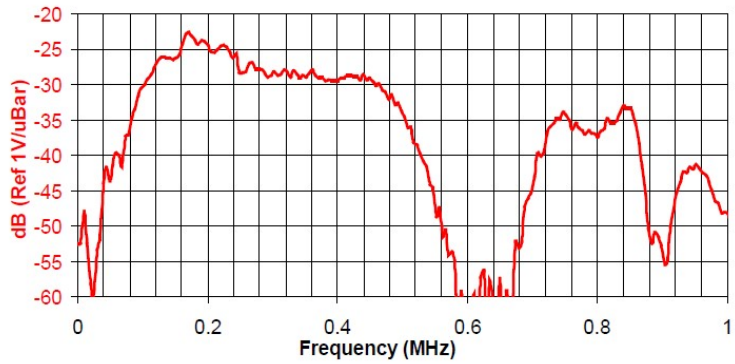

Figure 2.4. F15I AST wideband sensor response with 150 kHz peak resonant frequency shown in MHz

2.10. AE AND FRACTURE MECHANICS

The theoretical interpretation of energy balance of the system can be explained by a method following a Griffith approach to Fracture Mechanics. In this approach stored elastic energy is is accounted before and after damage

$$E_a = E_b + W - \Delta E \tag{2.3}$$

Where E_a is the energy after the system has reached an equilibrium and E_b is the energy before the stress. W is any work done by external forces and ΔE is a balancing term. ΔE is then defined as,

$$\Delta E = E_s + E_p + E_{AE} \tag{2.4}$$

Where E_s is the energy consumed in crack formation, E_p is energy given for plastic deformation and E_AE is the elastic wave energy released in the form of sounds (Carpinteri, 2010). Crucial in this discussion is the relationship between the elastic wave energy and accumulated number of Hits stated mathematically as

$$E_AE(t) \propto N_AE(t) \tag{2.5}$$

This relation was introduced by Pollock and Carpinteri and noticed in the testing performed in this study. In these circumstances we are considering this as a closed system without external noises or heat dissipation.

2.11. CRACK LOCATION DEVELOPMENT

With principals of mechanics and material properties of the concrete, an understanding of crack development within a concrete structure can be understood. Many different studies have looked at the location of cracks, crack orientation and type. It is of practical importance for estimating the damage level of structures. (Ohtsu, Okamoto et al. 1998) Researchers have sought ways to approach the subject with a high degree of sophistication to understand the development of crack growth. There are different levels of sophistication in determining location of an AE hit which are dependent on specimen geometry. There are of course simplified methods to obtain location information which rely on the principals of arrival times at each sensor location. The AEwin software which comes standard on the Samos AE System was developed to analyze 1,2,3 dimensional structures. This approach is based primarily on the differences of arrival times of AE

Hits. The math for this approach is shown. Where d is distance, v is velocity and t is relative arrival time between sensors

$$d = v * t \tag{2.6}$$

Signals will arrive at each sensor at different times based on travel distance. Knowing the wave velocity is important for accurate measurements. For each calculation, the relative time is taken as the difference in arrival times of the sound from the first sensor to the next sensor. Thus by determining the difference of arrival times and known coordinates of the sensors, it is possible to determine the location of AE Events as they are occurring in a material. For a one dimensional problem such as analyzing sounds generated on a cable structure or rather a structure with very large aspect ratios, the math is relatively simple because linear distance is a singular unknown. For 2 dimensional and 3 dimensional structures the math is much more difficult. Using Pythagorean Theorem expressed in Cartesian coordinates, the equations for two dimensional source location can be expressed

$$d = \sqrt{(x_2 - x_1)^2 + (y_2 - y_1)^2)} \tag{2.7}$$

$$t_2 - t_1 = (d_2 - d_1)/v \tag{2.8}$$

$$t_2 - t_1 = [\sqrt{(x_2 - x_s)^2 + (y_2 - y_s)^2)} - \sqrt{(x_1 - x_s)^2 + (y_1 - y_s)^2}]/v \tag{2.9}$$

This shows that in equation 2.9 with unknown coordinates of the source there are 2 unknowns and it cannot be solved by itself. To get a second equation with the same 2 unknowns, a 3rd hit is added to the event producing an analogous equation.

These equations can be solved simultaneously to determine the position of the source in terms of x_s and y_s. Troubles occur when there are variations of arrival times or when additional signals are captured simultaneously from other sources. Thus far more accurate locating algorithms have been written to perform regression analysis to minimize errors in the generated locations. Certainly more densely sensor populated arrays can provide more accurate information on the location of signals for structures tested. Having more recorded Hits, the equations for source location is expressed as

$$t_2 - t_1 = [\sqrt{(x_i - x_s)^2 + (y_i - y_s)^2)} - \sqrt{(x_1 - x_s)^2 + (y_1 - y_s)^2}]/v \tag{2.10}$$

$$\Delta t_i = t_i - t_1 \tag{2.11}$$

Applying a regression technique, the error is reduced by minimizing the difference between 2 quantities which are observed and calculated. The software developed by Physical Acoustics uses this approach to determine a reasonable location based on iterating potential values finding the least summation of values across all sensors recording the same event

$$\chi^2 = \Sigma(\Delta t_{i,obs} - \Delta t_{i,calc})^2 \tag{2.12}$$

The sum is recalculated for each potential source location. The location code will search for values of x_s and y_s to minimize the value for χ^2. The method the code uses is based two types of algorithms. The Simplex method is used for Planar Modes in 2D and 3D space and Powells Method is used for spherical, cylinder and conical locations. The methods for analysis obviously becomes challenging when the structure being studied is 3D or has a complicated geometry with discontinuities like embedded steel or joints. Having a vast array of sensors improves the capabilities of the technology for studying material degradation but possess some practical issues.

2.12. METHODS OF AE ANALYSIS

2.12.1. RA/AF. A method developed for classifying cracks into categories of tensile and shear based on four wave parameters. Risetime divided by peak amplitude and counts divided by duration (average frequency). This theory first outlined by the Japanese Construction and Material Standard is shown in Figure 2.5. As damage progresses, generated sounds will transition from tensile cracking sounds to shear cracking sounds. For most instances, it would be assumed that as cracks transitioned into macro cracks the rubbing due to translation would produce more shear crack noises. This theory could then be used to map crack propagation so it could be used to evaluate damage (Farhidzadeh et al, 2013).

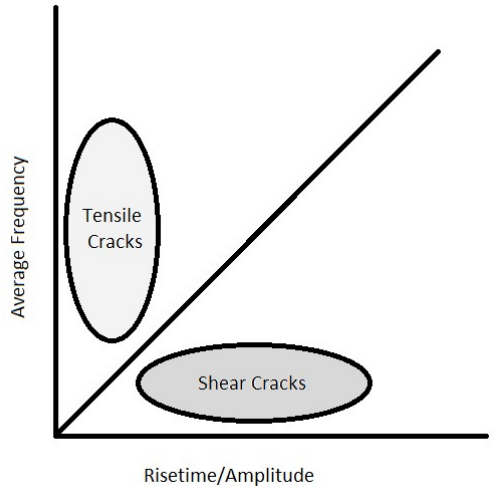

Figure 2.5. RA/AF Diagram For Tensile and Shear Cracking

2.12.2. Calm Ratio and Load. Many investigators have attempted to use AE parameters to quantify the damage level of RC structures. At least five such methods have been reported. One important damage assessment method is the correlation of calm ration and load. This has been developed into the standard of JSNDI 2000 (Yuyama, 2005). These methods of analysis can be applied to cases where cyclic loading takes place. The calm ratio is related to crack closure during unloading (Liu and Ziehl, 2009). The calm ratio uses the cumulative signal strength of unloading divided by the cumulative

signal strength during loading. The rate of damage assessment of concrete compression test of cylinders has been conducted by Ohstu and Watanabe, which corresponds to the micro cracking of the concrete. Their evidence shows that the presence of critical microcracks in concrete is closely associated with cracking behavior with AE generating behavior (Matsuyama and Ohtsu, 1992).

2.12.3. B-value. Proposed by Pollock in 1981 and modified by Ohtsu and Watanabe in 2001, Colombo et al. in 2003 and Farhidzadeh. The b-value method of establishing damage within a structure is based on a principals popular in seismology related to the Gutenberg-Richter equation corresponding to the magnitude of the Earthquake to the frequency of Events

$$log_{10}N = a - bM_L \tag{2.13}$$

Where M_L is the Magnitude and N is the incremental frequency with a and b as constants which are determined as properties of the material and test configuration. In this application, the equation will be modified by changing the b coefficient to match the data present. For AE research this equation is rewritten as

$$log_{10}N = a - b(A_{dB}/20) \tag{2.14}$$

Where A_{dB} is the recorded maximum amplitude of the signal and b is variable and a potential indicator of damage. What is observed during a test is as microcracking coalesces into macrocracking the frequency of the Events within a time increment decreases and the maximum amplitude of the event increases. In the work done by Colombo with reinforced concrete beams, it was seen that patterns arose from the b-value tracking the damage of a beam under a cyclic loading protocol. Because this beam was reinforced it was able to resist the brittle failure characteristic of concrete and also represent what would normally be seen in a real world application. In these tests, the calculated b-value has a very sporadic behavior. Generally, the b-value decreased through the microcracking

process, then sharply increased as microcracking transitioned into macro cracking, and finally decreasing at the onset of structural collapse.

This technique has been improved upon by Farhidzadeh and Salamone who have taken an involved approach to filter extemporaneous signals to form a desirable sample which is then modified using statistical and average techniques (Farhidzadeh and Salamone, 2012). The analysis of the selected b-values is necessary because of the many fluctuations in the b-value trend due to reflections, random crack orientation, and attenuation of the signal. This technique employed is known as Sifted b-value and can be used to help predict the stage of damage. The method developed by Farhidzadeh and Salamone involves an iterative procedure known as k-mean clustering. The method randomly clustered sets of signals and averages them to find a minima of the variance thus sufficiently grouping signals into the appropriate group. This group is than further analyzed using the smoothed b-value techniques.

This approach to understand the damage process on the global level takes a well understood principal and applies it to a rather complicated phenomenon with a nearly chaotic conclusion. Given the necessity of having to employ empirical constants, this method does have some draw backs but does provide an interest perspective on the issue of damage history with each given specimen.

2.12.4. Historical Index Versus Severity Index. This method of evaluation takes into account two different parameters in evaluating the damage of a concrete structure. This was originally applied to bridge structures and is defined by two different values, the Historical Index and Severity Index.

The historical index is defined as

$$H(t) = \frac{N}{N-K} \frac{\sum_{i=K+1}^{N} S_{0i}}{\sum_{i=1}^{N} S_{0i}} \tag{2.15}$$

Where n is the number of Hits up to and including time t, S_{Oi} is the signal strength of the i-th event and K is the empirically derived factor that varies with the number of Hits.

$$K = \begin{cases} 0 & \text{N} < 200 \\ 0.8\text{N} & 200 \leq \text{N} \leq 1000 \\ \text{N-200} & \text{N} > 1000 \end{cases} \tag{2.16}$$

Severity index is the other parameter used for this analysis and is defined as the average signal strength for the 50 Events having the largest numerical value of signal strength, mathematically it is represented by

$$S_r = \frac{1}{50} \sum_{i=1}^{i=50} S_{0i} \tag{2.17}$$

When plotted, these two values can represent damage within a structure by representing intensity curves showing the damage states of small defect, significant defect and major defect reaching a collapse. This approach has been applied to concrete structures but with the aid of supervised corrections to correlate reliable results.

2.12.5. Relaxation Ratio. Colombo et al. in 2005 as a possible means to assess the residual strength of RC beams. This method is based on the principle that the presence of AE energy during the unloading phase of an AE test is generally an indication of structural damage (Colombo, Forde et al. 2005). The relaxation ratio is also related to crack closure during unloading. The relaxation ratio is defined as the ratio of average signal strength during unloading to the average signal strength during loading. This differs from the Calm Ratio because the average signal is used in place of the cumulative signal strength.

2.12.6. Cumulative Signal Strength Load Ratio. Proposed by Ridge and Ziehl to characterize the damage level of CFRP-strengthened RC beams. This ratio corresponds to the Felicity effect. It is taken as the ratio between the cumulative signal strength during reloading divided by the cumulative signal strength during the previous reloading step.

2.12.7. Calm Ratio Versus Load Ratio. The aforementioned AE criteria can be applied individually as just described in this section; the load and calm ratios have

been used by the Japanese Society for Nondestructive Testing in to place the damage level into three separate categories, minor, intermediate or heavy (Ohtsu and Yuyama, 2000).

2.13. BRICK RESEARCH MOTIVATION

Bricks serve as a material of choice for modern day homes and institutions being stylish, durable, and historical. Bricks are generally of two types, fired clay or casted concrete. Both are used quite extensively in construction. For brick structures that are used as load bearing members, they suffer from a lack of ductility and lateral strength. During an earthquake, brick structures are likely to suffer significant damage, which has caused loss of life. Notably, after the great San Francisco Earthquake of 1906, most of brick structures were reduced to rubble. As a consequence of this natural disaster, structural engineers were tasked with redefining their approach to building design.

Over the past 100 years changes have been made to Concrete Masonry Units (CMU) which has improved performance. For example, the compaction of the concrete mix had evolved from hand compaction to machine compaction. For improving the material properties, researchers at Missouri S&T are investigating methods to make the material more ductile. Since it has similar crushing strain as concrete, a lot can be done to improve ductility. CMU bricks in this study have been prepared with a fine rubber aggregate to replace a portion of the sand content. The design aim of this research is to be able to produce a brick which is capable of withstanding a greater amount of strain without cracking.

3. MASONRY PRISM TESTS

3.1. INTRODUCTION

This research intends to use AE technology to monitor the damage progression in Concrete Masonry Units. Since CMU always works as a compression element, observing the effects of compressive stress while collecting AE is crucial for detecting and accessing damage. In this study, the loading of the specimen was chosen to represent forces caused by earthquake. It was expected that the nature of these sounds would change over time while using AE sensors collecting sounds. Six different CMU specimens were tested using AE while monitoring physical changes of force and displacement. Using a basic AE setup by equally spacing sensors on the specimen, several AE parameters were evaluated while the specimens were brought to failure. The evidence of damage was captured by observing the changes to important characteristics of recorded hits.

Behavior of bricks using AE has been studied by other researchers. Fracture of masonry has been investigated extensively by researchers at the University of Torino. Alberto Carpinteri, who published in the area concrete fracture mechanics, has studied the fracture process of masonry as it under goes various types of failures. Using a number of different SHM techniques, Carpinteri, Grazzini, and Lacidogna conducted static, creep and fatigue tests while monitoring performance. They studied both uniaxial compression and shear strength for both static and cyclic testing. Fatigue testing of masonry has been pursued by researchers such as Melbourne and Tomor, De Santis and Tomor, Masera et al. Carpinteri and Invernizzi who have conducted testing on vaulted ceilings and masonry arch bridges. In their research they have determined that masonry is quite vulnerable to fatigue damage in shear and compressive stresses much lower than that of ultimate (Carpinteri et al., 2014). In Carpinteri's study of shear fatigue loading of bricks, the behavior of the bricks strengthened with a mortar skim coat was tested. The strain is

defined by the strain curve in Figure 3.1 for cyclic load at 70% of ultimate (Carpinteri, 2014).

For this type of specimen which was cyclically tested at 70% of static capacity, the acoustic waves generated by the process can be characterized as a steady progression until the specimen reached a failure. Three different stages of damage; primary, secondary and tertiary phases are depicted in Figure 3.2 and correspond to strain of the specimen. The bold line represents the cumulative AE hits. This research shows that it is possible to monitor damage in real time.

Fatigue loading is often the case of structures subjected to high repetitive loads like that seen by bridges and towers made from brick. For the researcher, it is essential to distinguish between damage patterns and damage evolution leading to catastrophic structural collapse (Carpinteri et al., 2007).

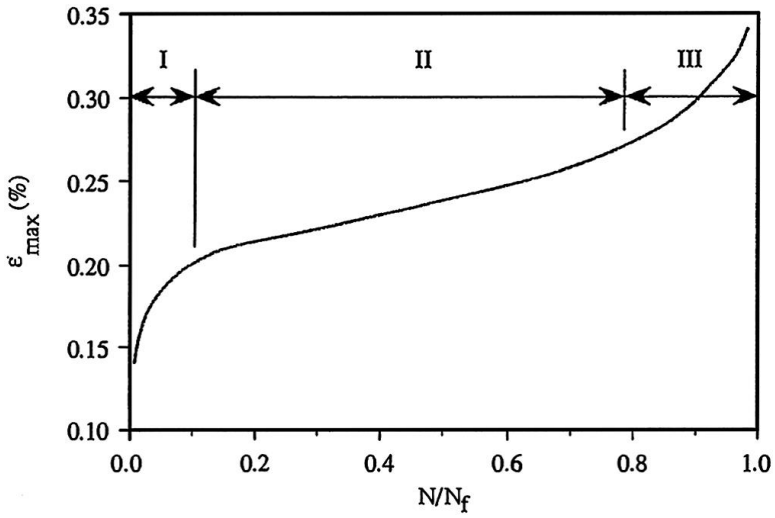

Figure 3.1. Masonry fatigue test cycle-strain relationship with three damage states (Carpinteri, 2014)

The b-value method has been used to categorize damage with masonry structures. The b coefficient in this process is mapped as an indicator of damage progression and has an inverse relationship to damage. Closer to material failure the lowest b-value could be registered. More information on this parameter can be found in Section 1.13.3. This

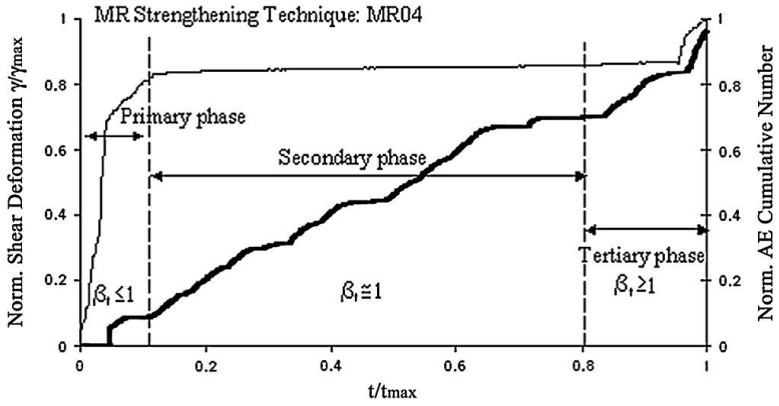

Figure 3.2. Masonry fatigue test cycle-strain relationship with three damage states (Carpinteri, 2014)

technique has been shown to match real observation on only a basic level due to a sizable deviation in each registered value. It is also necessary to define empirical constants based on material properties. The downside of this approach is even with evolved techniques of Gaussian smoothing it still lacks a physical certainty of accuracy, thus this approach was not pursed.

The monitoring technique used in this study aimed at observing several different parameters of the recorded data. From work done by Tomor who showed that in masonry there was an increase amplitude as crack progressed from micro to macrocracks, the peak amplitude of recorded waves was taken into consideration (Tomor and Versrynge, 2013). The number of times a recorded wave crossed a predetermined threshold (counts) was studied as a means to evaluate damage. As well as the frequency centroid, representing the weighted average of all of the frequencies in the spectrum of a single hit similar in concept to a mass centroid of a cross section. Mathemtically this is shown in equation 3.1. The AE software equipped with the Mistras Micro II is AEwin has a built-in ability to output this value. Last approach considered was effect of RA/AF over the time of the test. This concept is explained in the Literature Review. Given the unpredictable dynamic nature of damage evolution in CMU specimens, the approach in this study defines clear trends in detecting this damage in six unique brick specimens.

3.2. TEST SETUP AND SPECIMENS

3.2.1. Brick Specimens. A displacement step control was used to load the bricks until failure. The specimens tested were of four concrete masonry units (CMU). An S-Type Portland cement mortar was placed between each layer and in some cases the prism was filled with grout. The bricks tested had different amounts of fine rubber granule. The grout used was a high strength 5 ksi mix. A portion of the sand was replaced with a fine rubber aggregate. The given percentages were 9%, 19% and 37% weight of rubber replacing sand in the mix design.

The bricks were cast into a typical CMU shape, with two openings within the center of the cross-section. Only two of the specimens tested were fully grouted. The reference CMU and brick with the highest rubber content, 37% rubber incorporated grout. All of the specimens were allowed to attain a full working strength before testing. The masonry bricks were 15.625 x 7.625 x 7.625 with a 0.375 thick layer of mortar. Due to the similarity in brick appearance, a color designation is listed to help organize the test setup as it was performed. Date of the test was used to help organize data. The specimens tested along with their peak results are shown in Table 3.1.

Table 3.1. Text matrix

DATE	% RUBBER	COLOR CODING /GROUT
NOV. 11	37	WHITE/YES
NOV. 14	19	BLACK/NO
NOV. 17	0	NORMAL/NO
NOV. 18	9	YELLOW/NO
NOV. 19	37	WHITE/NO
FEB. 6	0	NORMAL/YES

3.2.2. Loading Configuration. A MTS 500 kip capacity load frame was used to conduct the uniaxial cyclic test. The load was spread by two inch thick steel plates, one connected to the actuator and the other placed on the base. These plates distributed the force of the actuators piston across the prisms cross section. The base plate was allowed to pivot so that adjustments could be made to correct the plum before the load was applied. On each end of the brick prism, a gypsum/fiber mat with a rubber laminate was used to help distribute the force from the plates. This helped minimizing stress intensities along the brick's edges. The mats also helped prevent any lateral shifting between the plate and the specimen. Information on the actuator's position and load were fed into the data acquisition system and stored with data from the LVDTs. Load was applied at a constant displacement of 0.02 in/min during loading and unloading. It was applied to the specimen in cycles at the given rate until the maximum increment was reached. The specimen was unloaded at the same displacement rate until the force on the specimen was zero. The specimen was then reloaded at the same rate until the same increment was reached. The cycles were continued in groups of 3 and then the peak increment was increased by 0.5 inches. Cycles continued until the specimen failed.

3.2.3. Sensor Configuration. The AE signals were collected throughout the test by 8 transducer sensors of two different types placed on one face of the specimen on a grid. The sensor location's spacing (see Figure 3.3) was kept constant so that the results were more accurate. An assembly of hot glued plastic angles attached the sensor to the surface. A pipe collar bundled the plastic angles to the sensors. To couple the sensor to the structure, a layer of grease were applied directly to the senor head.

The sensor parameters are listed in Tables 3.2 and 3.3. The threshold type was defined as floating. The floating threshold helps account for a high noise environment by raising the threshold by as much as 6 dB. The gain was set to 40 dB because it is a common setting for a preamplified sensor. The filters were set to higher levels to avoid recording unwanted noises. The length of the file was set so that it recorded the entire typical wave, a wave more intense than a pencil lead break.

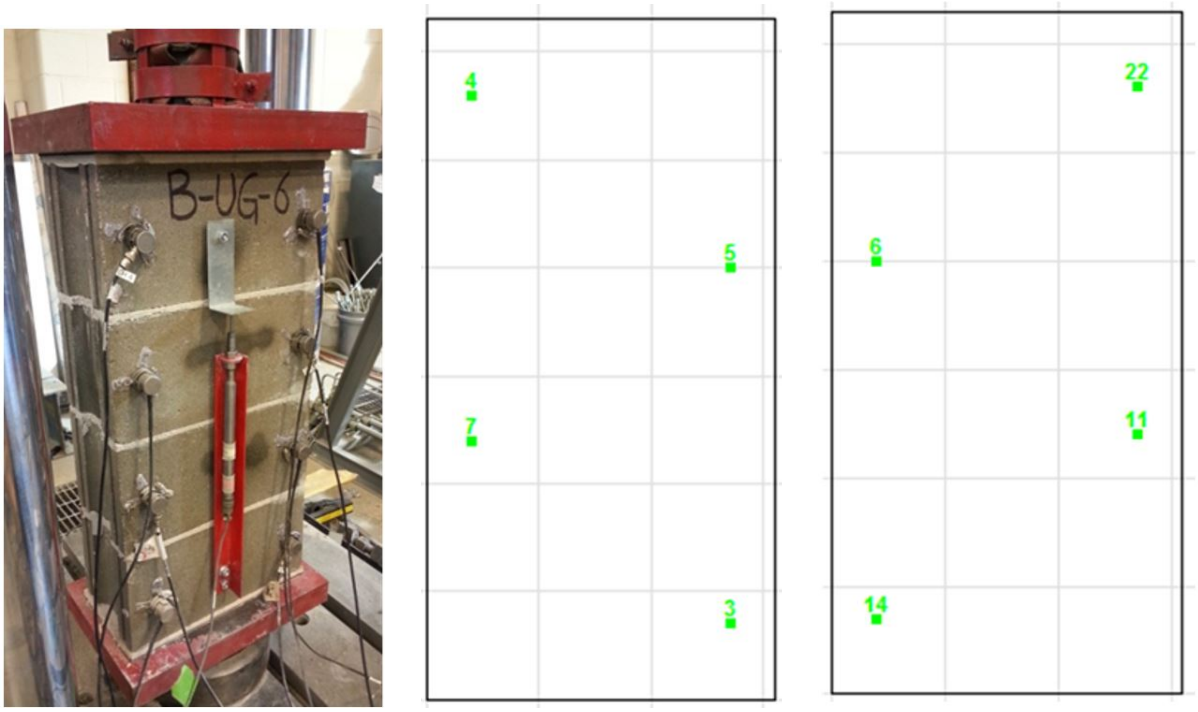

(a) Specimen (b) F15 Layout (c) R1.5 Layout

Figure 3.3. Sensor layouts and test setups of masonry prism tests

The peak definition time (PDT), hit definition time (HDT), hit lockout time (HLT) and Max Duration were set so that the software could accurately record the entire wave. Each was set to levels much higher than those found in literature so that the full signal could be recorded. This adjustment was made from observation.

A pencil lead test was performed to adjust the sensors threshold levels. These levels were held constant throughout all experiments. To calibrate the AE data with the load, a scaled voltage reading displacement was sent as a parametric from the MTS actuator control to the Micro II. This scaled parametric was used as a benchmark or refenerce in assessment. The AE sensors recorded every sound during the test above the designated threshold level and outside of the hit lockout time. The pre-trigger captured the head of the arriving wave. Wave parameters were amplitude, counts, signal strength, frequency centroid and RA/AF values.

Table 3.2. AE hardware parameters

Type	Threshold	Threshold	Gain	Low Filter	High Filter	Sample Rate	PreTrigger	Length
F 15 AST	Floating	42 dB	40 dB	20 kHz	400 kHz	3 MSPS	150	3k
R1.5 AST	Floating	48 dB	40 dB	1 kHz	200 kHz	1 MSPS	256	3k

Table 3.3. AE timing parameters

Type	PDT	HDT	HLT	Max Duration
F 15 AST	500 µsec	1000 µsec	100 µsec	1000 ms
R1.5 AST	1000 µsec	2000 µsec	1000 µsec	1000 ms

3.3. RESULTS AND DISCUSSION

3.3.1. Load Results and Discussion. Six specimens were tested. A DAQ system recorded measurements of the actuators force and displacement. The change in length of the LVDTs mounted on the front and back side of the specimen was recorded and these results are shown in Table 3.4 in terms of ultimate values or the highest values of these quantities.

Table 3.4. Masonry prism load results

% RUBBER	GROUT	ULTIMATE LOAD (KIP)	ULTIMATE ACTUATOR DISPLACEMENT (IN)	ULTIMATE DISPLACEMENT LVDT 1 (IN)	ULTIMATE DISPLACEMENT LVDT 2 (IN)	AVEARAGE LVDT DISPLACEMENT
0	NO	205.4	0.401	0.102	0.017	0.060
9	NO	130.8	0.401	0.026	0.132	0.079
19	NO	129.3	0.551	0.267	0.012	0.140
37	NO	55.1	0.501	0.402	0.011	0.207
0	YES	257.3	0.510	0.166	0.113	0.140
37	YES	239.6	0.952	0.244	0.332	0.288

Results of displacement and force of the actuator for the grouted specimens of normal bricks and brick with 37% added rubber are shown in Figure 3.4. Graphs of the displacement-time, force-time and force-displacement relationship for the six specimens are included in Appendices A1 thru A6. What can be seen in the force plots such as in Figures 3.4a and 3.5a is that for all brick prisms there is a reduction in structural

resistance after the completion of the first cycle of each step, this can be referenced in Appendix A1-A6. As noted by Carpenteri, bricks are susceptible to cyclic or fatigue at load levels below ultimate (Carpenteri, 2014).

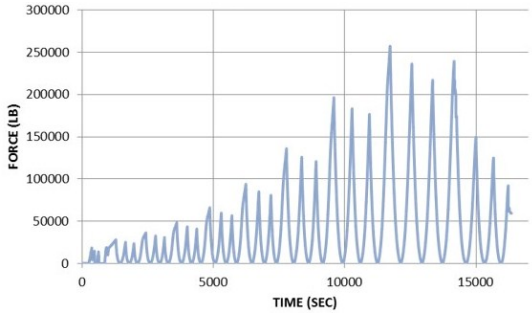

(a) Force-Time plot normal CMU grouted

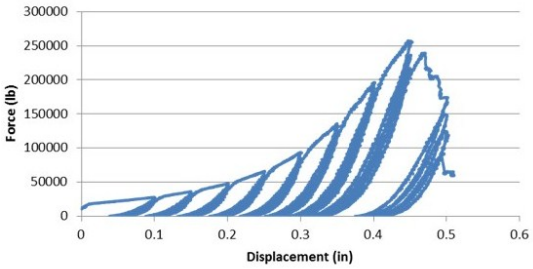

(b) Force-Displacement plot rubber CMU grouted

Figure 3.4. Normal CMU grouted load results

Two major benefits were identified in the rubber which can be seen in the force displacement relationship. The 37% rubber brick was able to endure more cycles of loading thus higher strain. In contrast, the normal grouted specimen (see Figure 3.4) suffered from a lack of stiffness and strength during the last complete cycle. The softening behavior can be seen in the plots of force and displacement in Figures 3.4b and 3.5b as the change in the slope of the force displacement curve. Interestingly, the slope of the last group of curves in Figure 3.4b is more shallow indicating the material softened. The

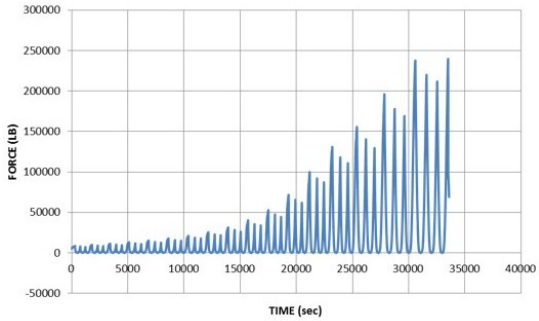

(a) Force-Time Plot 37% Rubber CMU Grouted

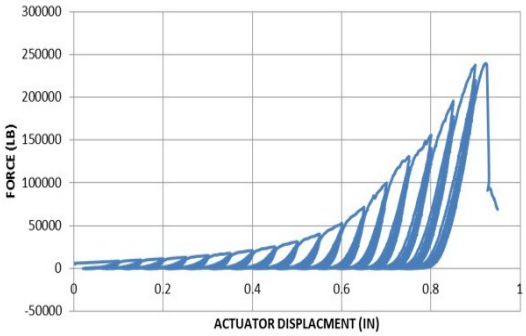

(b) Force-Displacement plot 37% rubber CMU grouted

Figure 3.5. 37% Rubber CMU prism grouted

last loading cycles step for the grouted rubber sample (see Figure 3.5a) didnt diminish. The impact of replacing a portion of the sand aggregate with a fine rubber particle on the strength was investigated. The specimens that were grouted had significantly more strength than the un-grouted specimens as was expected. In observing the strengths of the bricks such as the grouted and un-grouted 37% (white) specimen, the addition of rubber decreased the overall strength. Grouted specimens with 37% rubber had 20% less strength. The 37% rubber specimen had 4 times the strength when grouted but the most noteworthy observation is the effect of the rubber on displacement of both actuator and LVDT displacements.

Having a frame of reference such as displacement is essential to help understand the behavior of the cracking. The specimens' fracture pattern was of interest in this study. The AE sensors were applied to monitor how the specimen was damaged fulfilling the main objective of damage detection. Location was pursed in this research but there were many errors in the position of recorded events by the AEwin software, so the approach was abandoned. The rubber specimens did not break apart in shards; the increased ductility allowed for greatly energy dissipation. Figures 3.6b, 3.7d and 3.7c shows that large pieces of brick broke away. This behavior did not occur with the rubber brick. The areas that did fail, did so when the material was crushed. This failure mode appears to have been more localized, reducing crack propagation.

Concrete with rubber added is far superior in material ductility. Looking at displacement results of instruments, by averaging the LVDT displacements in Table 3.4 for the normal grouted specimens and number 37% rubber averaging grouted CMU prism, it can be seen that the rubberized grouted specimen had 3.4 times the amount of displacement and the sample had 2.5 times more LVDT displacement over the normal CMU. The experimental setup allowed for rotation which prevented strain build-up on one side due to an uneven bearing surface. Damage accumulated and the material initially softened after each cycle. Plastic deformation occurred after each loading step (see Figures 3.4b

and 3.5b because the displacement corresponding to zero force shifted from the initial position).

Vertical cracks formed at midsection of the width and depth dimensions, where the compression stress was the highest. Tension stresses developed transverse to the line of compression within the brick due to the Poisson Effect. These cracks propagated into large macrocracks that lead to failure at hairline crack locations. It can be seen that the behavior of the brick differed. In Figures 3.7c and 3.7d the normal CMU cracked throughout every side. Large shards of brick broke away from the grout core. Due to the rapid release of energy, some of the reference CMU simply blew apart (see Figure 3.6b and Appendix A8). The bricks with 37% rubber did not have the same vertical crack formation, instead horizontal shear cracks appeared at the location of high stress at the uppermost brick.

A number of differences in structural behavior between the rubber CMU and the normal CMU should be noted. In general, the strain was significantly greater before strength loses with the rubber specimen, which is more desirable for material ductility especially in earthquake design. Bricks with rubber were also able to release energy at a slower rate. Thus sudden crack propagation was not as severe. The large vertical cracks in the normal CMU were a direct result of sudden energy release. These cracks propagated throughout the prisms entire height thus creating major stability issues.

3.3.2. Acoustic Emission Results. Results are shown based on hits analysis of individual sensors and sensor group behavior related to the two sensor types used. Individual sensor behavior differed in each sensor group. Sensors located at the bottom of the specimen did not record as many hits as those located close to the top. Each individual hit is shown in the amplitude, counts and time plots of the entire R sensor set, illustrated in Figures 3.8 and 3.9. These distributions were conducted with a signal threshold of 50 dB.

The actuators displacement is included in these plots to give a frame of reference. The results show the effect of hits, signal strength, amplitude, counts, and average

(a) 37% Rubber CMU Ungrouted

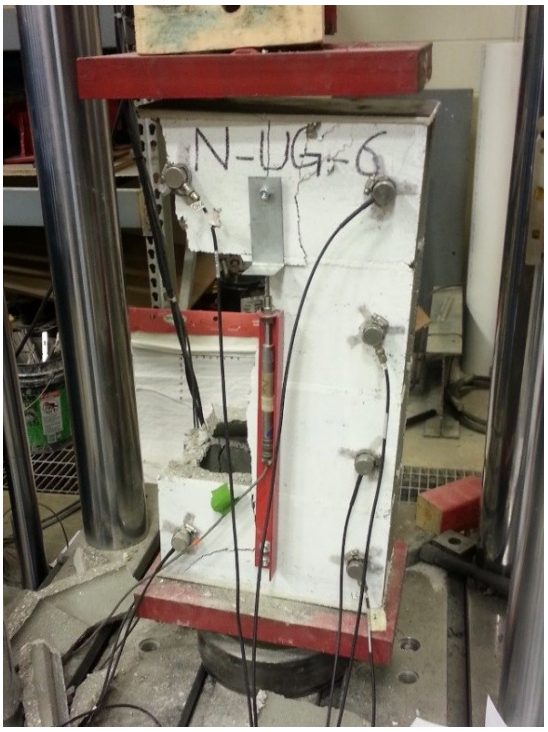

(b) Normal CMU Ungrouted

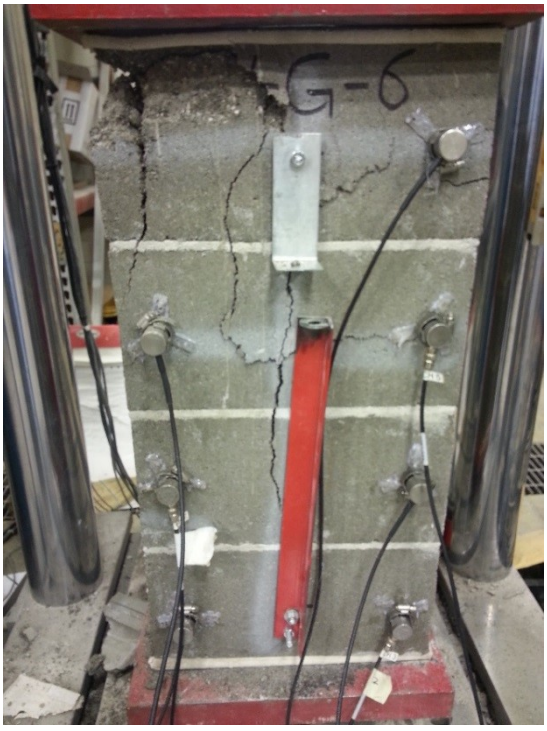

(c) 37% Rubber CMU Grouted

(d) Normal CMU Grouted

Figure 3.6. Damaged specimens with and without grout from the completion of cyclic test with and without Rubber

(a) Backside of 37% Rubber CMU

(b) Edge of 37% Rubber CMU

(c) Edge of Normal CMU

(d) Back Side of Normal CMU

Figure 3.7. Damaged grouted specimens from completion of cyclic test with and without rubber and grout

frequency centroid over time within each test. Since experiments were conducted with grouted specimen, those results are shown as another set of data. Included in this analysis is a risetime/amplitude versus average frequency plot also represented in the temporal domain.

Acoustic Emission was effective at detecting cracking as it occurred. The progression of damage corresponds with a release of energy in the form of sound waves. This energy is proportional to the number of recorded hits (Carpinteri, 2010). A sudden release of energy (see Figure 3.14) corresponded to new cracking at the peaks of new load steps. This behavior can be identified by a steep slope of the Hits over time. In comparing the results of the brick with and without rubber. The bricks with rubber recorded less Hits. In comparing the results of the two sensors, the higher frequencies were attenuated by cracking and the material properties of the brick, because there is a significant decrease in recorded hits by the F sensor when rubber is added to the mix. In comparing the signals from the R sensor which is a low frequency AE sensor, the recorded Hits are less but within the same magnitude. However as previously noted in the physical behavior of the bricks with rubber, the cracking behavior differed. Cracks that formed in the specimens did not progress as rapidly; hence less recorded Hits.

In these tests it was impossible to avoid capturing reverberations or reflections of sounds. The Hit Lockout Time was increased to avoid this problem but given the small thickness of each brick, sounds bounces rapidly off of the surfaces. Also multiple hits were recorded with the file duration thus nullifying some of the AE hit parameters such as wave length, PDT, HLT and HDT. The risetime of individual waves could be misrepresented and the counts parameter would account not just to one waveform but several. These kinds of errors are unavoidable because by shortening the max duration or length of the recorded wave a lot of the waves features will be lost.

A lot of unknowns play a part with the behavior of the recorded parameter. Reflections of sound waves were due to interfaces between bricks and the thickness of the brick. A rather basic approach of looking at the peak amplitude of the waveform, and the

number of times the waveform passed a threshold (counts), there were some interesting trends. Plots of amplitude and counts over time, Figures 3.8 and 3.9 and Appendices A13, A14, A17 and A18 reveal that significant structural damage produces signals with a high amplitude and counts.

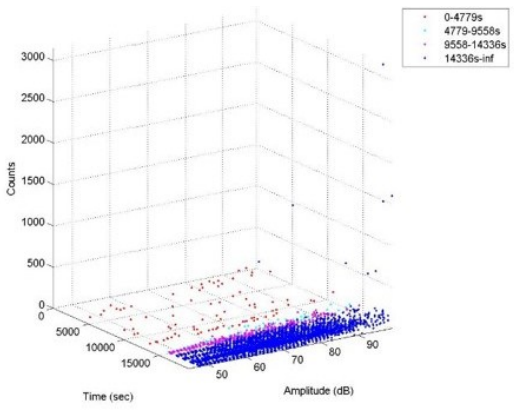

(a) Normal CMU Ungrouted

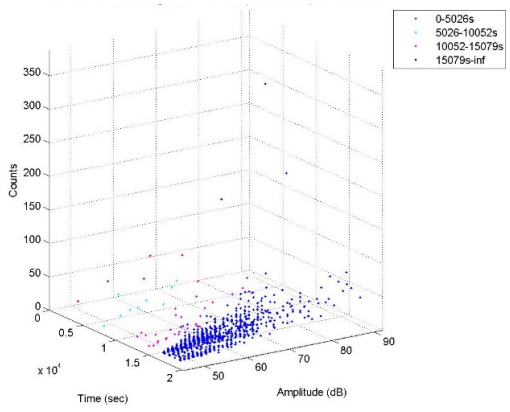

(b) 37% Rubber Ungrouted

Figure 3.8. R sensors ungrouted specimens amplitude-counts-time

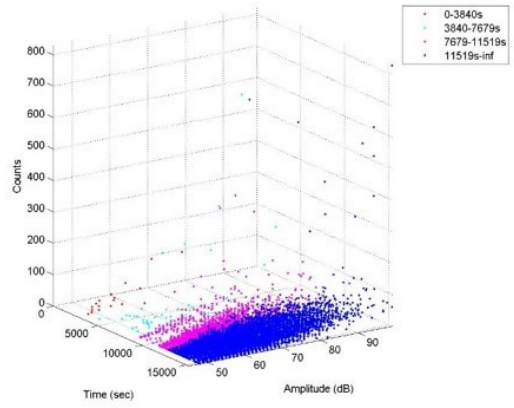

(a) Normal CMU Grouted

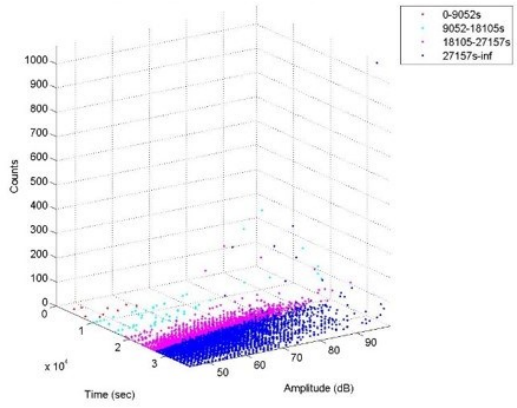

(b) 37% Rubber Ungrouted

Figure 3.9. R sensors grouted specimens amplitude-counts-time

These findings correlate with when the force was reaching the peak of each cycle. The counts in these plots followed a similar trend. A higher number of counts was generated when a significant force was applied. Due to the energy stored as strain, the sudden release through cracking produced many signals with a high number of counts. It seems appropriate in observing the amplitude and counts because it captures the

continuous signals which are sometimes represented as outliers related to points of major damage.

Two different sensors were used in this study. In general, a large number of AE hits were released at the peak of a new load step which can be seen clearly as a steep slope in Figures 3.10b and 3.11b.

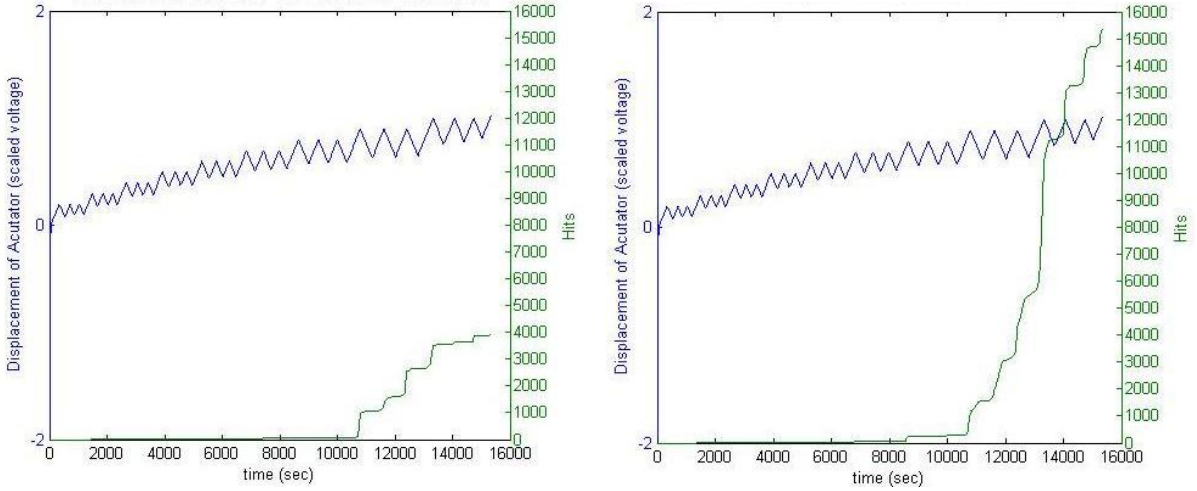

(a) F Sensor (b) R Sensor

Figure 3.10. Normal CMU Grouted cumulative hits

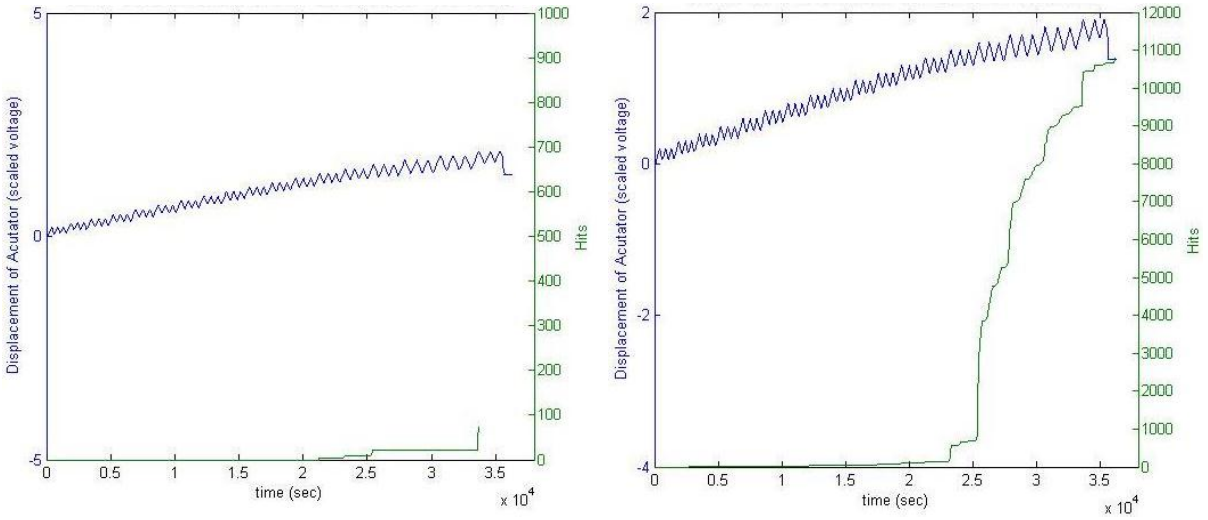

(a) F Sensor (b) R Sensor

Figure 3.11. 37% Rubber CMU grouted cumulative hits

In general, by comparing the results of the grouted and ungrouted specimens, many more R sensor hits were recorded with grouted CMU. An indicator of damage is the reduction of F sensor hits and the increase of the R sensors' hits. This trait can be identified in these figures and also by comparing the results shown in Appendix A22. These plot hits for both the F and R sensors simultaneously. It was expected that the damage within the structure would attenuate higher frequencies only recording lower frequencies.

An approach taken by Ohtsu and Farhidzadeh is to evaluate RA/AF. Which are the parameters of the risetime divided by the peak amplitude and the average frequency of the individual signal. This method has been accepted by the Japanese Society of Nondestructive Investigation and was used to examine the behavior of cracking. The results are shown in Figures 3.12 and 3.13 and Appendices A15 and A19.

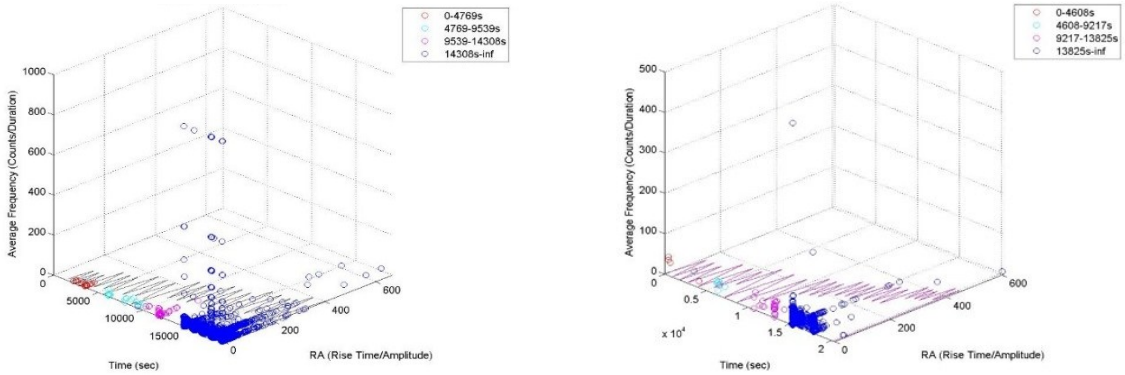

(a) Normal CMU ungrouted (b) 37% Rubber CMU ungrouted

Figure 3.12. RA/AF Plot R Sensor Group ungrouted

With this approach, signals that lie in the vertical axis correspond to tensile cracks. Signals along the horizontal axis are related as shear dominated. As might be expected, a tensile crack would be caused by a dilation of the compression plane due to the Poisson effect. Grinding between crack surfaces occurred when the existing cracks opened and closed. These new cracks should be registered as shear cracks. The results of these tests showed otherwise. Signals that were at the extremes occurred in

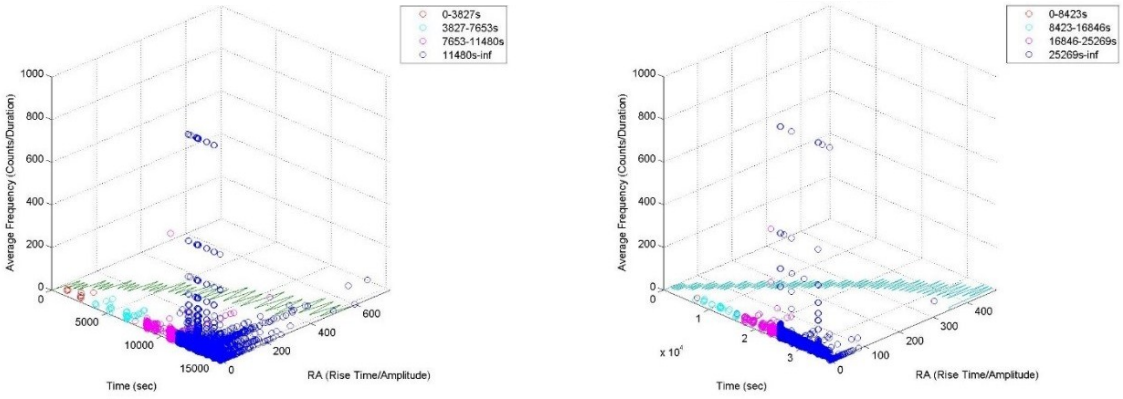

(a) Normal CMU grouted (b) 37% Rubber CMU grouted

Figure 3.13. RA/AF plot R sensor group grouted

both axes occurred simultaneously which does not seem to follow an expected behavior. Outliers appeared at instances where significant cracking occurred. More than likely these outliers were continuous waves resulting from a high number of recorded signals collected simultaneously at moments of significant energy released as a result of a large applied force.

Signal strength is another important indicator of the specimens behavior. Cumulative signal strength plots are given in Figures 3.14 and Appendix A21, cumulative signal strength plots have been included to show how damage has increased throughout the test for each individual sensor. The signal strength as previously noted, is the integral of the rectified waveform, given units of pico volt seconds. Waves were collected during loading and unloading phases, when there was a significant applied force. The signal strength was always higher at high levels of load and displacement with a larger amount of energy released due to the formation of new cracks.

To keep track of the sound waves which are proportional to released energy, the graphs have been cumulated, this creates a better frame of reference in comparing results from an entire test. Sudden increases in energy correspond to the sudden release of sound waves. New cracking events usually occurred during larger load steps. In looking at Figures 3.15 and in Appendix A24, there are some obviously similarities between the

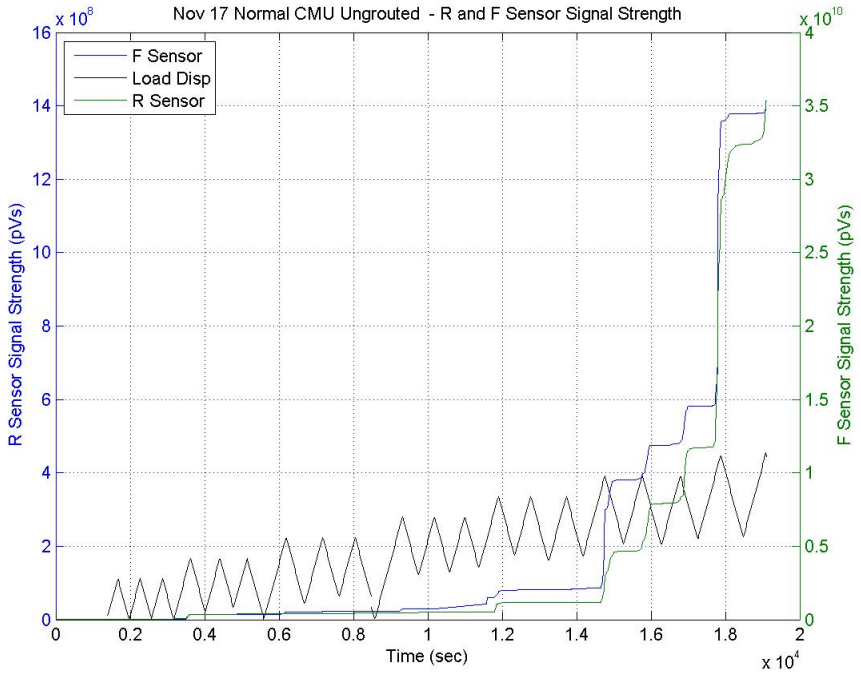

Figure 3.14. Normal CMU ungrouted R and F sensor cumulative signal strength

cumulated hits and signal strength for the R sensors. This agrees with the notion that elastic wave energy released by cracking is proportional to recorded hits. From studying all of the plots it appears that fewer cumulated hits corresponded to a smaller cumulated signal strength. The specimens that had a larger rubber content showed the highest attenuation of frequencies in the upper spectrum. This finding can be seen in plots that compare both the two sensors hits in Figure 3.14 and in Appendix A23. The ungrouted normal CMU had the least attenuation. Both types of sensors collected sounds at the same given moments in time, which is represented by the shape of these curves (see Figure 3.15). The signal strength is a relative term because specimens without grout seemed to produce higher signal strength. Comparing specimens in Appendix A23 this came as a surprise, since it would be expected that a grouted specimen would have cracked more surface area thus accumulated more recorded damage. One possible reason for this behavior was the higher amount of sound reflections from the small element thickness.

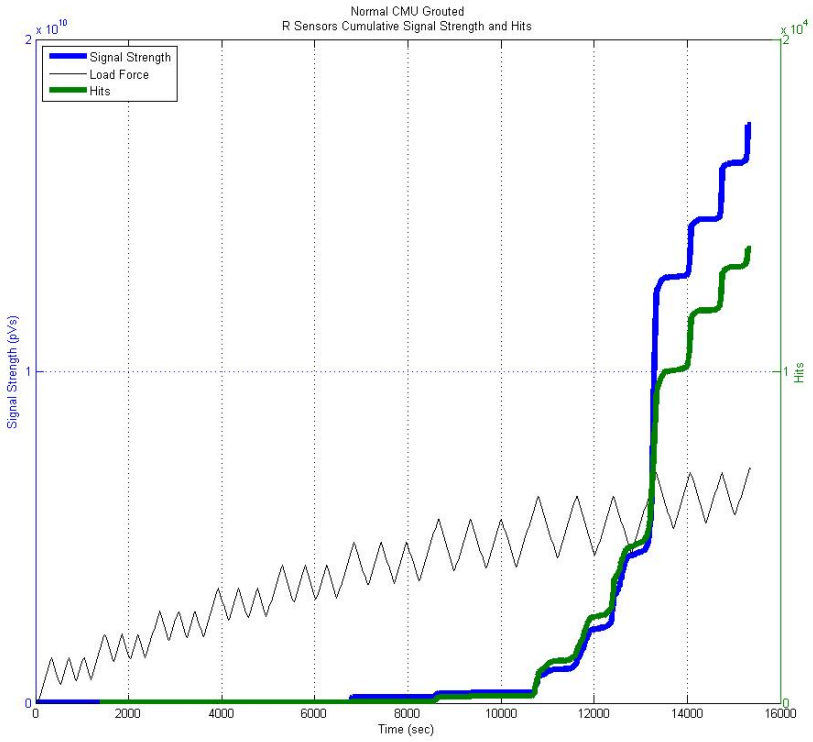

Figure 3.15. Normal grouted cumulative signal strength and hits R sensor group

The average frequency centroid was studied, these plots are of different sensors during the same test showing the average frequency centroid throughout the test of individual sensors. The average frequency centroid was created using AEwin over the time interval of 20 seconds. The frequency centroids of individual hits is shown in equation 3.1.

$$Frequency\ Centroid = \frac{\sum_{i=1}^{N} f(n)x(n)}{\sum_{i=1}^{N} x(n)} \tag{3.1}$$

where N is the total number of bins, n is the bin, $f(n)$ is the frequency and $x(n)$ is the magnitude or amplitude of the bin. The frequency centroids of individual hits are scattered. These figures show the data sets with a moving average and an error bar with the standard deviation of the sample set of each complete displacement step. The beginning of each plot starts at 50 kHz because of the format of the plotting technique. The grouping of the displacement step is meant to help assist in the analysis, determining

any noticeable patterns in the change of the frequency as the cracks were developing. When analyzing the results of the average frequency distribution an interesting behavior existed between the two sensors. The R sensor was in general better at capturing the behavior of decreased signal frequencies at the onset of failure shown in Figures 3.16 through 3.19. Frequencies of the F sensor were not as likely to show this trend as can be seen in Appendices A25 and A26. The results of the R sensors at the end of the test clearly showed a decrease in the frequency centroid from 30 kHz to 18 kHz for channels 6, 22 and 11 with a standard deviation of less than 3kHz.

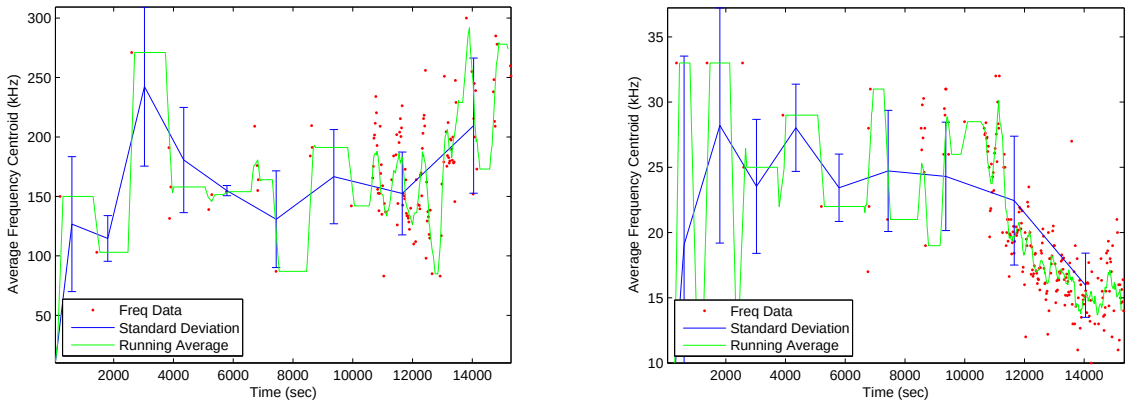

(a) F Sensor: Channel 5 (b) R Sensor: Channel 22

Figure 3.16. Average frequency centroid of individual channels normal CMU prism grouted

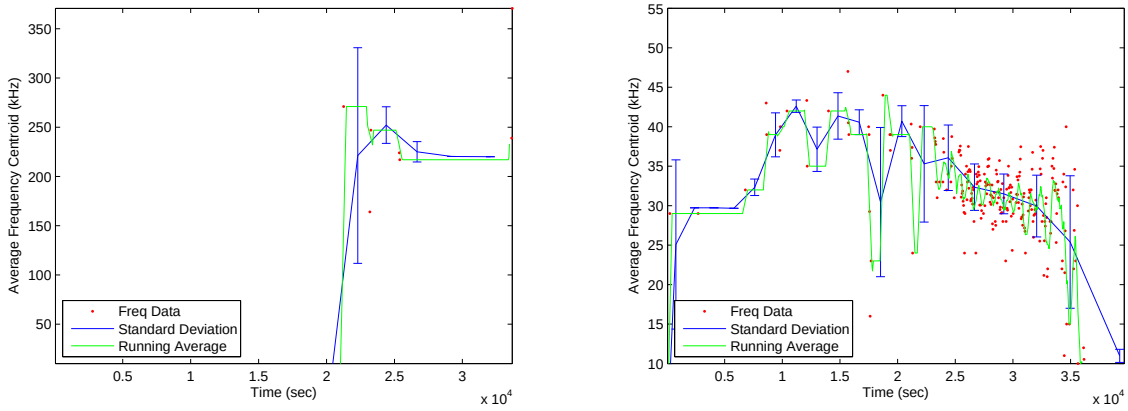

(a) F Sensor: Channel 5 (b) R Sensor: Channel 22

Figure 3.17. Average frequency centroid of individual channels 37% rubber CMU grouted prism

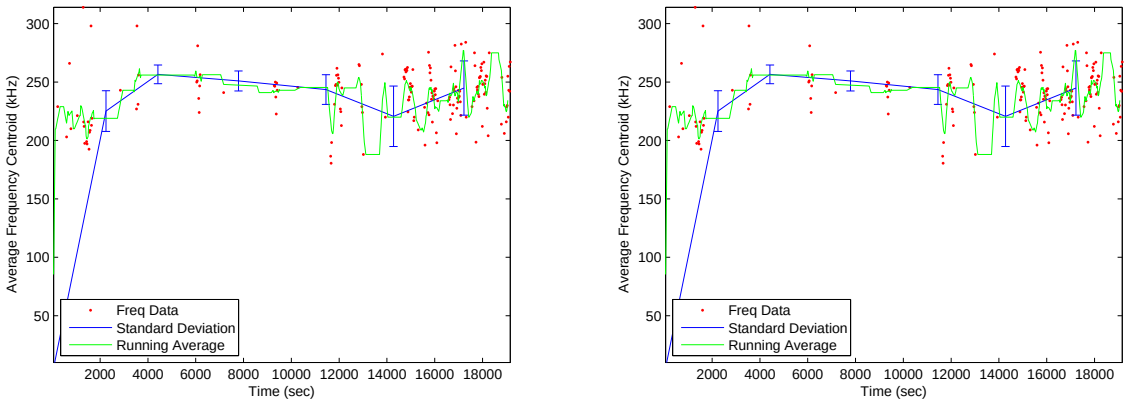

(a) F Sensor: Channel 5 (b) R Sensor: Channel 22

Figure 3.18. Average frequency centroid of individual channels normal CMU ungrouted prism

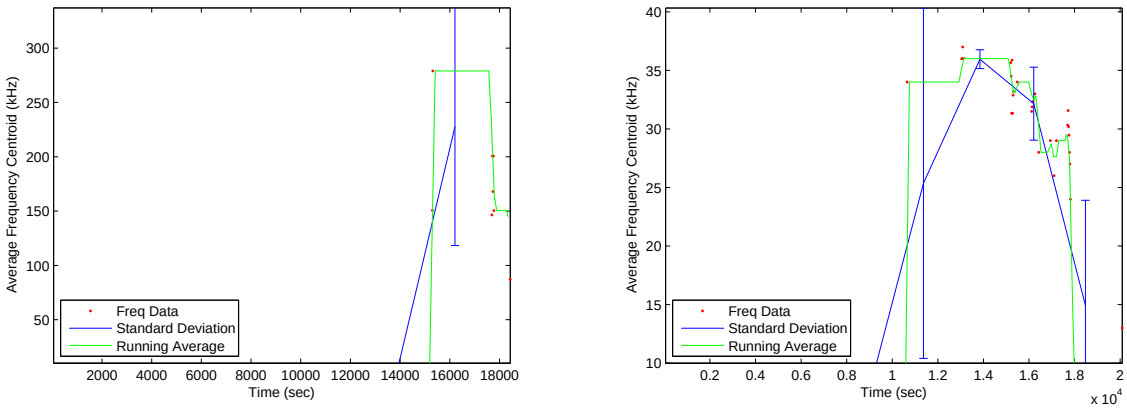

(a) F Sensor: Channel 5 (b) R Sensor: Channel 22

Figure 3.19. Average frequency centroid of individual channels 37% rubber CMU ungrouted.

In observing the connection between force and the frequency centroid of the recorded signals, the decrease of frequency does correspond to a decrease in capacity of the structure, it can be seen in Figure 3.20, clearly R sensors 11 and 22 are corresponding to when the brick spalled off. The closing of cracks would produce sound waves as would be expected. In the work done by Liu and Ziehl, who studied these quantified cyclic loading values using load relaxation ratio, and calm ratio, it was expected with cyclic loading that sounds would be gathered during loading and unloading cycle (Liu and Ziehl, 2009). When new cracks were created during loading, higher frequencies were

on the front of each step of damage. In comparing the results of the two specimens, after significant damage, the normal grouted CMU had broken apart into shards. The AE reflects more of a random frequency behavior with this specimen. It can be seen at points of reduced load there still were many signals recorded due to the sounds of large cracks closing. The damage of this specimen can be seen in Figure 3.20 and Figure 3.21. The 37% rubber grouted CMU retained more of its integrity so there is a clear omission of signals at zero force as well as less general randomness of frequency centroids.

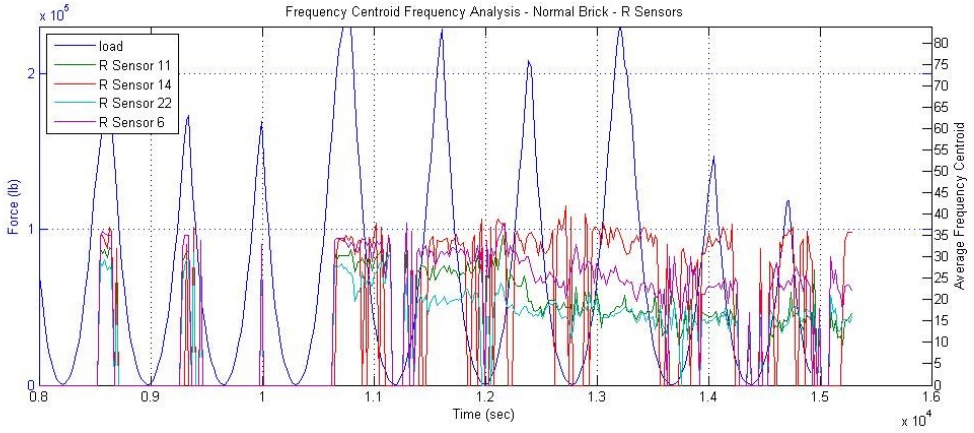

Figure 3.20. Average frequency centroid of R sensors and force (lb) for normal CMU grouted

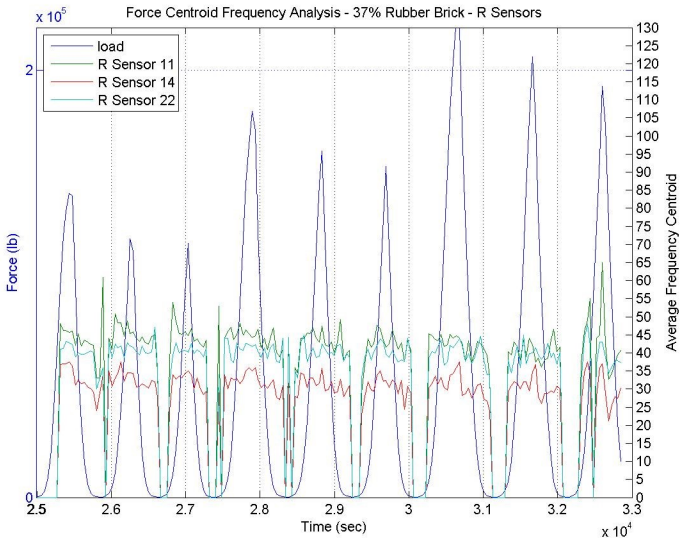

Figure 3.21. Average frequency centroid of R sensors and force (lb) for 37% CMU grouted

3.4. CONCLUSION

Compression tests were performed on a variety of masonry prisms following an incrementally increasing step pattern. The different prisms made use of various quantities of rubber with and without grout. During these tests, acoustic emission sensors were used to monitor cracking. To help understand the behavior of this new type of brick, a number of other monitoring techniques were used, LVDTs, actuator extension and force and video. Major findings of this study are listed:

- The R sensor (low frequency sensor) was better at capturing a frequency shift from damage. Major shifts in frequency are a direct result of damage to the specimen. A decrease in the number of hits recorded by the F sensor would be correlated with a higher degree of damage. At moments when no force was present, zero hits were recorded by either sensor.

- There was a noticeable increase in R sensor hits over F sensor hits as the damage to the specimen became severe. This is a good indicator of eminent failure because it clearly shows that new damage is progressing and that the existing damage is significant because of attenuation of higher frequencies.

- The benefit of using two different types of sensors was the ability to study the behavior of the frequency content of the recorded waves and have an understanding of the attenuation of brick due to damage. It was determined from the different materials tested that the impact of the rubber reduced the number signals recorded. The specimens with rubber recorded less hits, which maybe more closely related to material attenuation than the formation of cracks.

- To monitor the damage of the structure the amplitude and counts of individual waves were studied. It was seen in each test that as the specimen began to suffer from significant damage, the amplitude and counts both increased significantly. The largest amplitude signals were recorded at the peak of each cycle.

- In looking at the cumulative hits graphs, the moments with significant cracking resulted in a steep slope of recorded hits, which was always coupled with a new displacement step.

- The cumulative plots were good at showing the accumulated damage; however, signal attenuation occurred when rubber was added. For the specimens with the most rubber added, micro cracking at lower load levels was attenuated thus the crack initiation phase was captured at the start of each new step. Specimens with 9% and 19% added rubber cracked earlier on, the 9% had the highest signal strength of all of the specimens tested but it should be noted that these values are all relative. The F sensor recorded signals throughout the test of the grouted rubber specimen which would indicate that microcracking occurred at relatively low levels of stress.

- A RA/AF study was conducted and it was determined that there was no clear behavior from observing theses values. Outliers of these values would correspond to significant cracking events such as the first peak of a new load step. Shear cracking due to crack opening and closing was not well represented in this approach.

- The addition of rubber reduced the strength of the brick but greatly improved the ductility. With the addition of grout, the loss of strength was around 20%. The failure of the rubber brick was more ductile meaning that cracking did not propagate as rapidly, thus the material behavior during failure was more controlled. It was seen that the post peak strength of the brick was improved because of the materials energy dissipation properties.

4. SHEAR WALL TEST

4.1. INTRODUCTION

Masonry shear walls are a common building element in multistory structures. These walls are used to provide lateral resistance to forces produced by winds and earthquake. Their structural integrity is important in buildings to ensure the safety of occupants. Higher standards apply to certain facilities such as hospitals, school or places of commerce. Serve damage to these structures could carry grave consequences. A method of interpreting information from a technical point of view is necessary to better understand the actual state of unknown damage.

The Applied Technology Council has been providing resources to develop an engineered approach to not only a reliable warning system but also methodology for evaluation since 1973. The ATC-20 is a document that addresses the need for both a rapid and detailed evaluation procedure for structures damaged by earthquake. A full understanding of this damage can greatly enhance structural assessments after a devastating event.

This study captured damage to a shear wall as a result of extensive lateral movement. Testing was performed on two different shear walls with different configurations of post-tensioning rods. The interest in post-tensioning on masonry shear walls was to relate the lack of information on the design strength of masonry walls with an unbonded reinforcement. The Masonry Standard Joint Committee (MSJC 2013) treats post-tensioned masonry shear walls that do not include bonded reinforcement as unreinforced masonry walls due to limited experimental data available on PT-MW (Gheni and Elgawady, 2014). The behavior of these elements needs to be considered so that adequate information can be provided when revising design codes.

Acoustic Emission (AE) sensing is a viable technique for monitoring structures. The technology can be integral with the structure and provide real information about the

progression of damage. A sensing system could be incorporated for an extensive period of time that would provide a picture of a structure's health. The data collected could be used to draw a clear link between the AE activity that takes place and the damage that occurs. Incorporating several post-processing techniques, it is possible to develop a more accurate representation of a structure's damage that might be unattainable from visual inspection.

Two full scale CMU wall specimens were studied as the walls underwent cyclic in plane lateral loading. These tests were to simulate the kind of forces present when masonry shear walls are subjected to forces resulting from earthquake. The walls incorporated post-tensioning systems which effected their structural performance. AE sensors were used in these studies for damage detection. The design of these walls resemble what might be encountered in real building design. Using a similar approach in the masonry prism tests, information was gathered from two different types of sensors. This information was based on the changes of the characteristics of AE Hits throughout the stages of damage.

The goal was to understand through sound, the phases of damage caused by cyclic loading until the specimen failed. This research correlated global damage of the shear wall and material failure during the observed conditions of shear wall displacement. The failure mechanism involved toe crushing, sliding of the wall across the foundation and eventual rapid shear crack propagation. The approach taken was similar to the masonry prisms study by incorporating the same techniques of analysis. Due to the size of the member being tested, a significant number of sensors were applied to monitor the spread of damage as it progressed by way of cracking. Similarly, this approach used the same two types of sensors but in this case they were applied to specific regions were damage was expected to progress. From the results of this research, it is possible to incorporate AE sensors in real projects to evaluate the actual performance and give structural engineers a better understanding of the risks of damaged structures to health and safety of occupants.

4.2. TEST SETUP

4.2.1. Wall Specimens. Two walls were tested with two different post-tensioning configurations. A running bond pattern was used to construct the masonry shear walls. Each wall was fully grouted with 8-inch nominal concrete masonry units (CMU). An image of the setup is given in Figure 4.1.

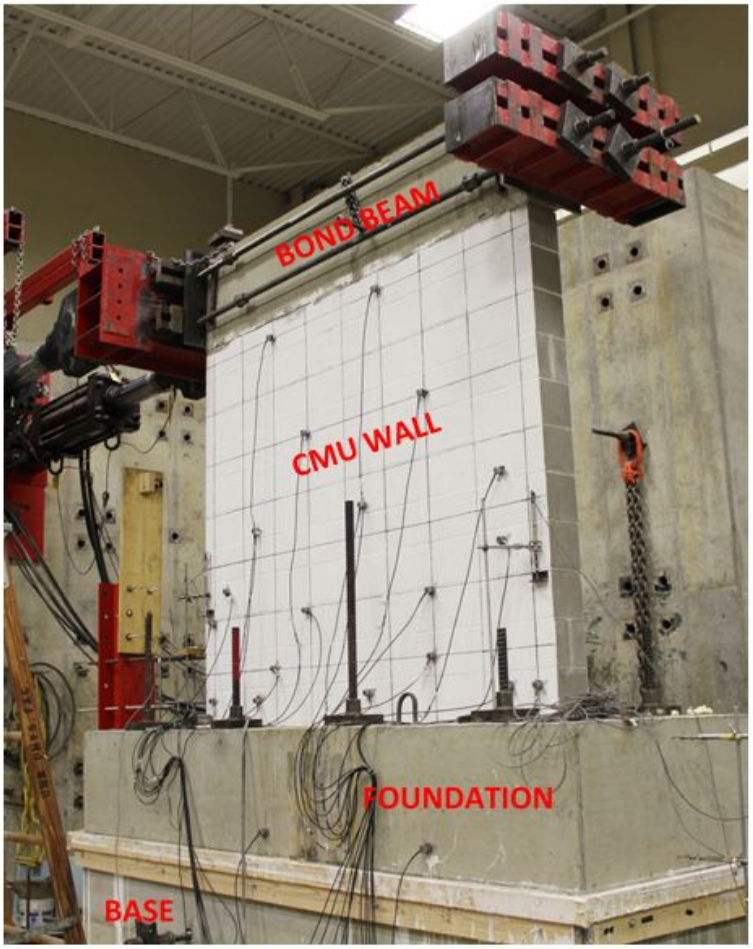

Figure 4.1. Masonry shear wall setup showing components

A high strength 5 ksi grout was used throughout this study. Between blocks, a Type S Portland cement-lime mortar was used. These walls did not have conventionally bonded flexural reinforcement but were post-tensioned with 1" diameter Dywidag grade 150 DSI post-tensioned rods. The end rods were tensioned to 30 kips, and the inner rods used in the first test were tightened to 45 kips. A stiff horizontal bond beam was attached to the top of the wall. This beam did not significantly improve shear capacity.

The wall was secured to the floor through a rigid foundation anchored with steel rods. Slippage was addressed by connecting the shear walls base to the foundation and strong floor with 8 Dywidag bars. The interface between the base and foundation was not even, so a layer of Hydrostone, approximately 1" thick was poured to distribute the force of the tightened rods evenly. The lateral force was applied directly to the bond beam with two 200 kip actuators in a north/south direction. These actuators were mounted onto a 2 foot thick concrete strong wall. Displacement was measured by the actuators and linear variable differential transformers (LVDT) located at critical points on the specimen.

A data acquisition system (DAS) was used to collect all data from instrumentation simultaneously. A Samos Mistras Micro II was used to capture AE of cracking of the brick. Video as well as still shots were taken to visually connect damage with AE data. This visual data was very useful in tracking the amount of damage for analysis purposes. Two different types of AE sensors were used in two different configurations. These configurations utilized the behavior of sound propagation and attenuation to provide insight into the unexpected structural behavior.

4.2.2. Acoustic Emission Approach to Analysis. This study addressed some of the most basic parameters of sensor output to avoid some of the shortfalls of complex analysis. From research done in the area of Gutenburg-Richter b-value analysis of shear wall AE testing by Farhidzadeh, cyclic loading by Liu, Z. and P. H. Ziehl as well as research done by Carpinteri with fracture mechanics and brick, it seemed logical to have a simple approach because of the many unknowns. It was accepted that the sensor data was gathered from random phenomena and the best approach was to look at the individual sensor behavior as well as lumping sensors into groups based on location and type. Observing the sensors' performances in this manner could also help evaluate the success of the technology's implementation due to the lack of repeatability. The approach of looking at some of the most basic AE parameters was similar to the analysis used in the masonry prism study.

4.2.3. Loading Configuration. Specimen loading was determined as displacement control protocol according to a cyclic procedure. This procedure increases the peak displacement of each step after two complete rounds. The loading rate for the test was kept constant according to FEMA 461. The step-wise increasing peak increment was given by the equation ai+1 =1.4ai with two complete cycles for each stroke. The rate of displacement was held constant at 0.03 inch/sec during loading and unloading. The walls were tested until they were unstable, thus leading to out of plane movement. Loading of the severely damaged wall had the potential to cause damage to the testing equipment.

4.3. SENSOR CONFIGURATION

4.3.1. Masonry Shear Wall One (four post-tension rods). This sensor configuration optimized the capabilities of the two different sensor types. The sensors' placement was based on their ability to detect signals within a theoretical radius. Signal attenuation is a challenge in large tests. Therefore, the sensors were placed in a manner that helped rectify this limitation. A higher frequency sensor was spaced around each of the toes of the wall's toes where microcracking was expected to originate (see Figure 4.2).

The sensor's spacing was crucial for location detection algorithms built in to AEwin. The spacing of the sensors was kept relatively constant for each sensor group anticipating that crack location could be investigated later on. The Figure 4.2 for Shear Wall One with 4 post-tension rods identifies sensor locations. For the first test setup, it was assumed that most of damage would result at the toes and potentially a diagonal shear crack would propagate across the entire length. Guard sensors were utilized but it was observed that their performance may not have been entirely effective at eliminating outside noise of the environment.

Selecting the correct sensor setting was extremely important in analysis of sound waves. The sensor profile required two different calibrations. The lower frequency sensor acquired more signals from a greater distance.

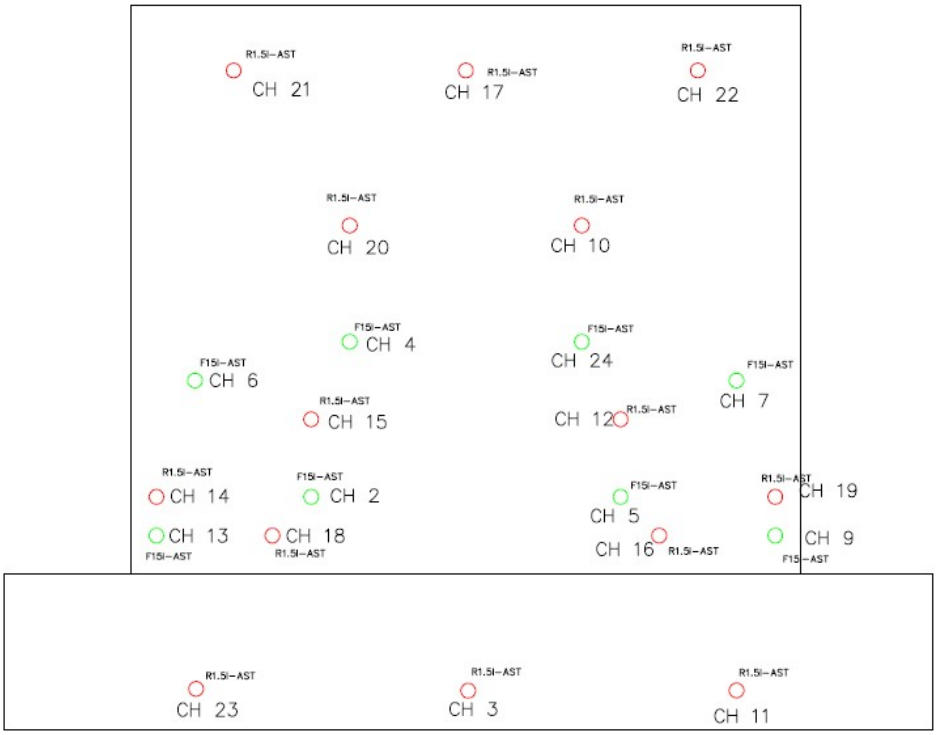

Figure 4.2. Masonry shear wall one sensor layout, where red circles are R sensors and green circles are F sensors

To compensate for this acuteness, the threshold was increased to help cancel outside noises. The timing parameters of the sensor was extremely important, the pre-definition time, hit definition time and hit lockout time were finely selected with to effectively record signals with clear distinct waveforms. The settings selected for these two sensors are shown in Tables 4.1 and 4.2. A little more treatment had to be taken into consideration, it was noted that many of the signals were in the lower frequency bandwidth. Adjustments of the wave file saved size, max duration and sampling rate were important so that full waves could be recorded. The issue of aliasing in this study was not considered, thus the sampling rate of the software was kept low and to help compensate for the unknown behavior of the system. Hundreds of signals were entering into the system nearly simultaneously. It was believed that the computers performance might suffer when tasked to record and store such a large amount of information.

Table 4.1. Shear Wall One AE hardware settings

Type	Threshold	Threshold	Gain	Low Filter	High Filter	Sample Rate	PreTrigger	Length
F 15 AST	Floating	45 dB	40 dB	1 kHz	400 kHz	500 KSPS	200μsec	1k
R1.5 AST	Floating	45 dB	40 dB	1 kHz	50 kHz	200 KSPS	256μsec	3k

Table 4.2. Shear Wall One AE timing parameters

Type	PDT	HDT	HLT	Max Duration
F 15 AST	750 µsec	1500 µsec	1000 µsec	1000 ms
R1.5 AST	750 µsec	1500 µsec	1000 µsec	1000 ms

4.3.2. Masonry Shear Wall Two (two post-tension rods). The sensor layout of the R sensors in the second shear wall was slightly different from the first. The array of R1.5 sensors was a grid pattern. (see Figure 4.3). The sensor spacing was kept constant because it could not be anticipated either where the shear crack would originate or what path it would take. A sensor layout that was needed so that the data could be analyzed statistically and could anticipate an indeterminate crack pattern. Based on the AEwin manual's location analysis, having an equally spaced sensor array will help the location algorithm converge through a sufficient number of iterations. A 2-D location algorithm was used. The results showed a high degree of uncertainty as damaged progressed, so they are not presented.

The F15I AST sensor was utilized in the zones where cracking and damage would initiate and populate extensively. This targeting revealed that the bricks fractured as the damage became more extensive. The use of two sensors offered additional insight into the crack's behavior as each crack transitioned from microcracking to macrocracking and, finally into material crushing. The hardware settings for the second test are shown in Tables 4.3 and 4.4. The hardware settings are slightly different with longer HDT, PDT, and pre-trigger to capture the entire wave. An LVDT layout was utilized in both tests to measure the wall's local movement. Each LVDT was positioned at a point where

movement was expected to occur. These results were not studied extensively in this analysis.

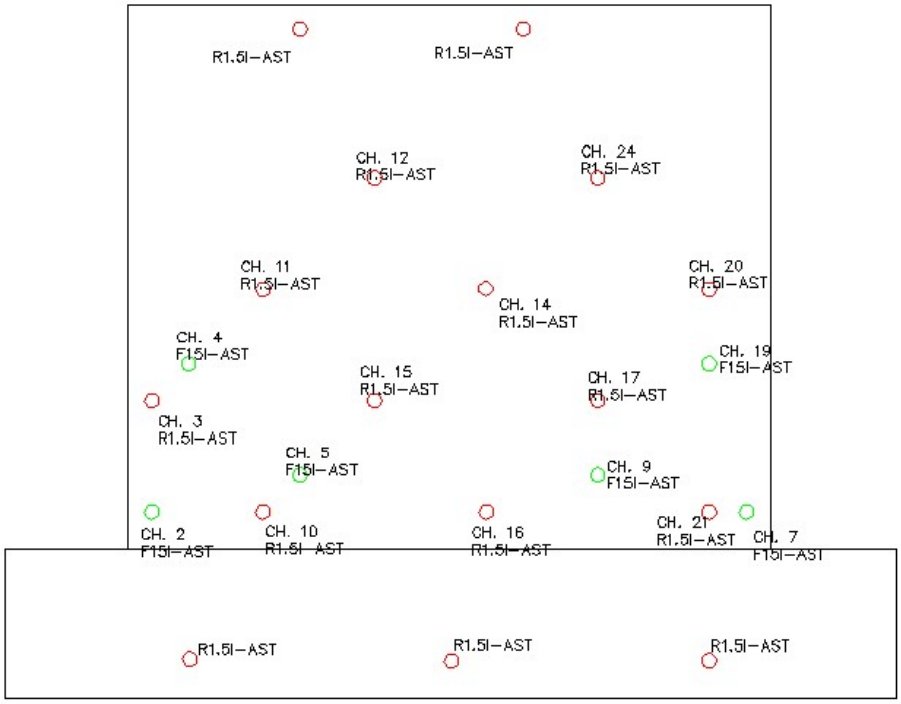

Figure 4.3. Shear Wall Two sensor layout, where red circles are R sensors and green circles are F sensors

Table 4.3. Shear Wall Two AE hardware settings

Type	Threshold	Threshold	Gain	Low Filter	High Filter	Sample Rate	PreTrigge	Length
F 15 AST	Floating	45 dB	40 dB	20 kHz	200 kHz	500 KSPS	300	1k
R1.5 AST	Floating	45 dB	40 dB	1 kHz	50 kHz	200 KSPS	500	2k

Table 4.4. Shear Wall Two AE timing parameters

Type	PDT	HDT	HLT	Max Duration
F 15 AST	750 µsec	1500 µsec	1000 µsec	1000 ms
R1.5 AST	750 µsec	1500 µsec	1000 µsec	1000 ms

4.4. RESULTS AND DISCUSSION

4.4.1. Load Results Masonry Shear Wall One (four post-tension rods).

Both walls were tested cyclically according to the prescribed loading protocol. The actuator's displacement over time for the first wall with four post-tensioned Dywidag bars is given in Figure 4.4. Figure 4.5a represents force of the pushing and pulling behavior of the wall up until the wall could no longer be pushed. Structural stability decreased with material failure. Figure 4.5b shows the complete force displacement relationship for the entire loading.

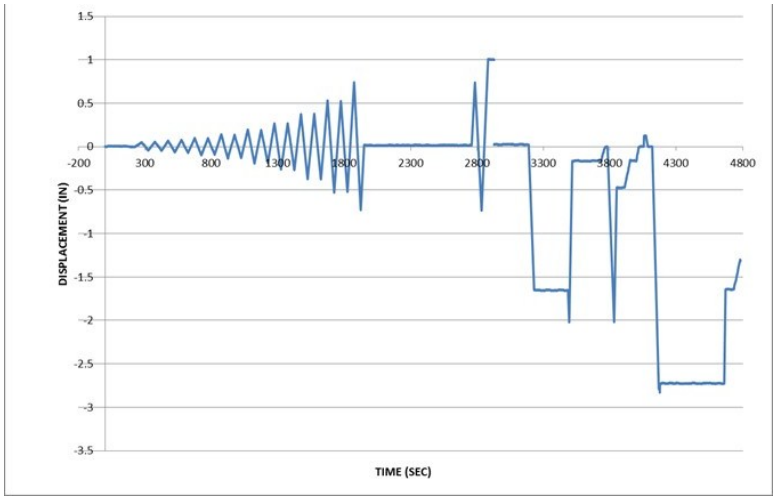

Figure 4.4. Actuator displacement applying force to the shear wall

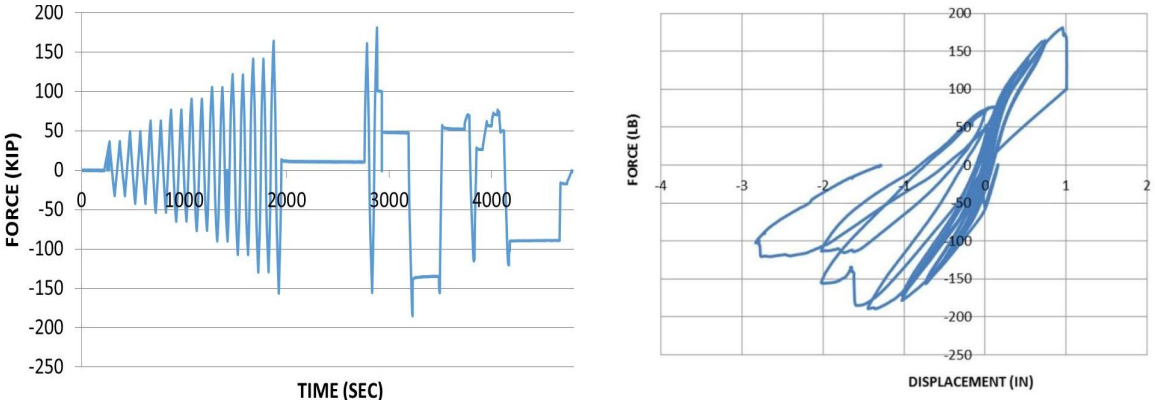

(a) Force-Time (b) Force-Displacement

Figure 4.5. Shear Wall One load results

A large diagonal shear crack propagated spontaneously as the wall reached a peak displacement of 2.8. This crack can be seen in Figure 4.6. Extensive damage can be seen in both of the walls' toe areas as those areas were subjected to large amounts of compressive force. It should be noted that the wall's damage was primarily related to the wall's compressive force as it was rocked back and forth. From visual inspection, the wall behaved as a rigid body instead of as a flexural member because of the lack of fixity at the base. As the wall was rocked in the north/south direction, compression built up at the toe in that particular direction as the other toe separated at the bed joint. The tensile forces that occurred due to the cantilever action was resisted by post-tensioning. The effect of the additional post-tensioning was additional frictional force between the wall-foundation and higher stiffness seen in the scope of the load hysteresis.

Figure 4.6. Shear Wall One damaged (the shear crack is indicated in green)

The material cracked at the toe of each side when in compression. The brick's failure mechanism involved material dilation. Crack formation occurred perpendicular to the line of compression. The vertical crack began propagating at the end of the wall. It continued propagated until larger areas of brick were cleaved off, because this material was weaker. The damage propagation at the toe on the north end of the Shear Wall One

is illustrated in Figure 4.7. The AE sensor had to be removed because it could no longer adhere to the surface as the damage increased.

The first sign of cracking occurred at the end of the wall and progressed as the strain became more significant (see Figure 4.7a). The material properties were different for each wall because each was a composite of concrete masonry, mortar and grout. The

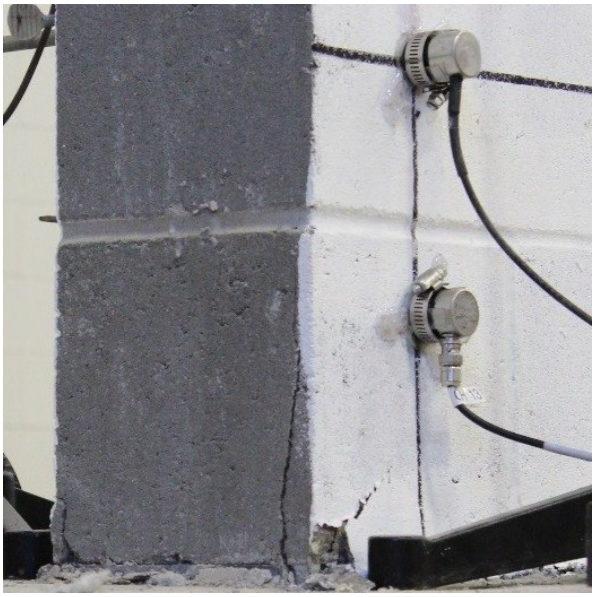

(a) Stage one

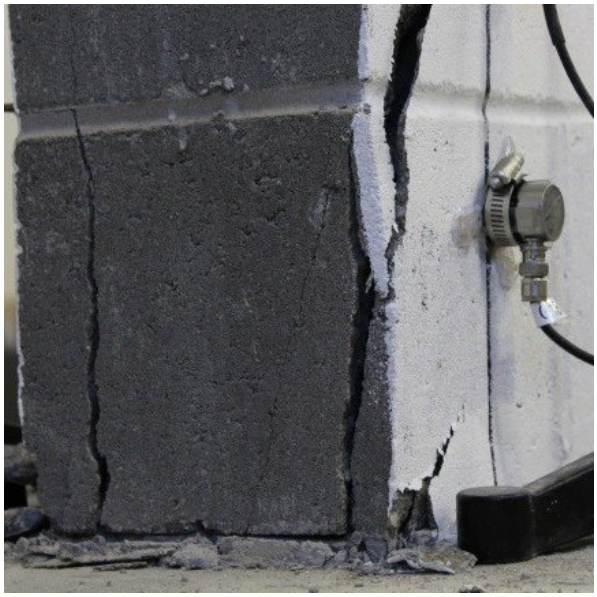

(b) Stage two

(c) Stage three

(d) Stage four

Figure 4.7. Shear Wall One damage progression at north toe

concrete masonry failed ahead of the grout as large chunks spalled off. This damage did not follow a particular pattern. It also failed to crack along joints between bricks as was predicted.

4.4.2. Load Results Masonry Shear Wall Two (two post-tension rods). Shear Wall Two with two post-tension rods followed the same loading profile as the first wall. The actuator's displacement over time of test are illustrated in Figure 4.8. The testing was paused to attach a crane to the specimen and then resumed. Just as in the previous experiment, there was more damage on the north end. The largest step was a pulling movement putting this toe into compression. In looking at the force of the actuators in Figure 4.9a it can be seen that the resistance of the wall was not as high as the first test. The softening behavior can be seen clearly in Figure 4.9b as the damage progressed. This behavior would be optimal in most designs because of the energy absorbed correlated to a larger area bounded by the hysteresis. A significant amount of sliding occurred between the wall and the base. Noises created by friction should be considered during this analysis.

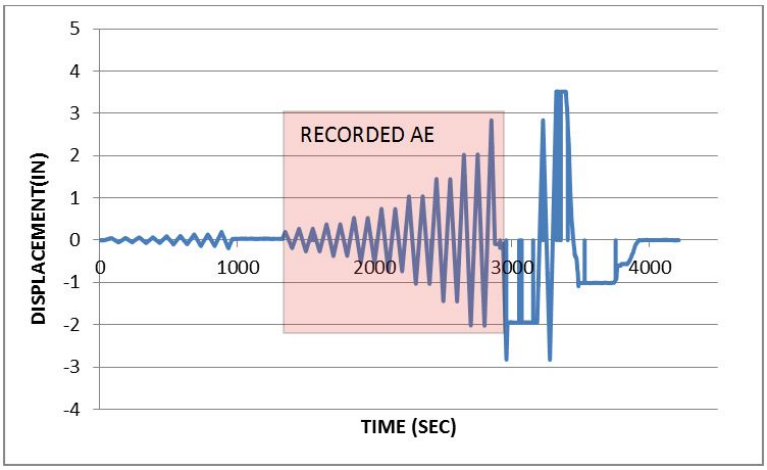

Figure 4.8. Displacement of actuator applying force to the shear wall

The wall's final state at the conclusion of the test is illustrated in Figure 4.10. The wall's peak displacement was increased. The PVC tubes are exposed in Figure 4.10 which reveals the location of the shear walls debonded rods. The damage at the toe of

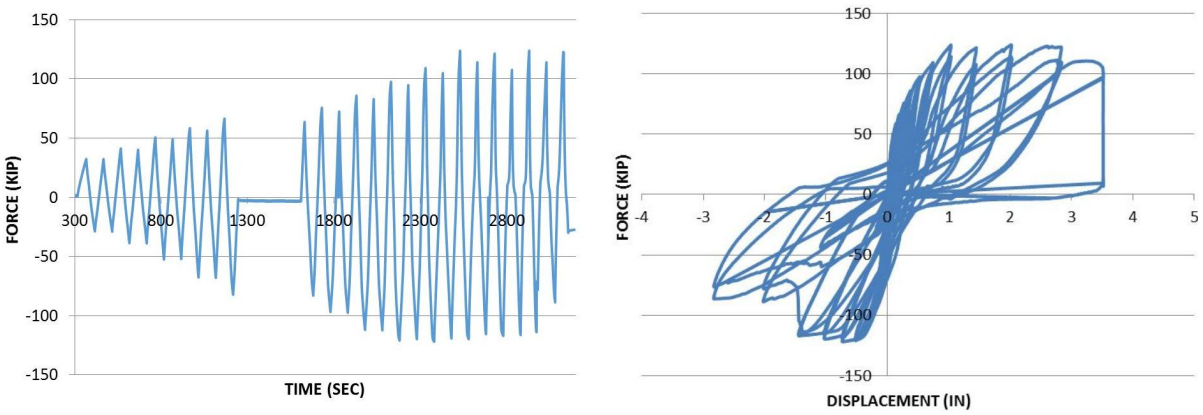

(a) Force-Time (b) Force-Displacement

Figure 4.9. Shear Wall Two load results

the wall is consistent with the previous test. The wall's rocking can be seen in Figure 4.11a. The toe in tension seperated from the base at the bed joint, this separation is shown in Figure 4.11a. In Figure 4.11b the cracking behavior was quite similar between both walls. The cracking at the toes began as vertical cracks and progressed until there were significant brick spalling and grout crushing.

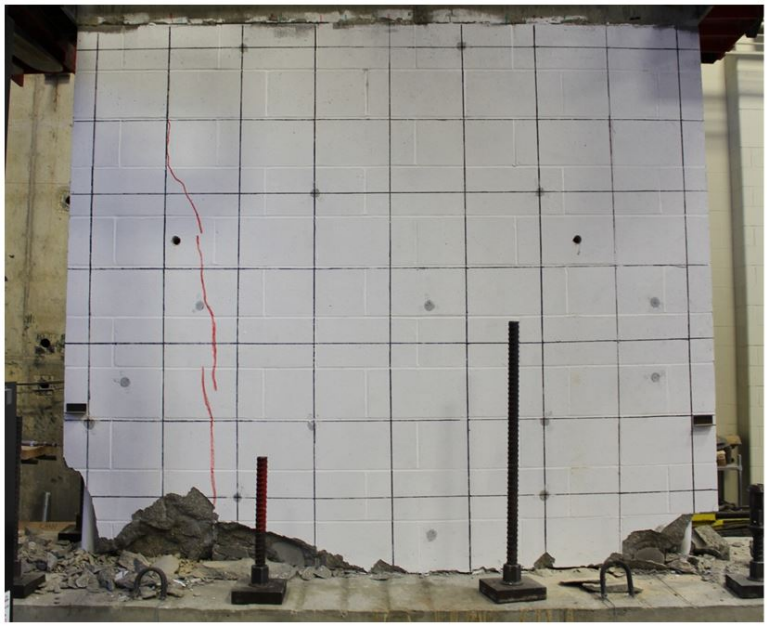

Figure 4.10. Shear Wall Two damage (vertical shear crack shown in red)

(a) Separation at the Bed Joint (b) Spalled Brick

Figure 4.11. South side of Shear Wall Two

4.5. ACOUSTIC EMISSION RESULTS

4.5.1. Shear Wall One. The sensors were able to sense cracking and also to determine the extent of damage before it was visually apparent by registering Hits. In capturing AE data, the output from the actuators was a frame of reference in correlating damage.

To help simplify the vast amount of data from these tests and reduce noise effects, the sensor data from each sensor was grouped together and given a higher a uniform threshold of 50 dB. All signals above 50 dB were analyzed. The grouping was based on sensor type and location. The locations of the sensors are illustrated in Figure 4.2. The organization for the group is shown in Table 4.5.

Table 4.5. Shear Wall One sensor group

Side	Type	Ch.	Ch.	Ch.	Ch.
North	F	6	4	13	2
North	R	15	14	18	
South	F	24	7	5	9
South	R	12	16	19	

The cumulative number of Hits for groups of sensors is shown in Figure 4.12. The groups were located in specific toe areas. The scaled force output from the actuator is represented as the blue line. These plots are a good representation of the damage on the wall, the plots are for both the north and south sides. The force readout has been flipped to show the negative values as positive when representing the north side of the wall. The sensors captured the wall's microcracking stage. This stage refers to low amplitude short bursts signals collected by both sensor types. The Hits detected in both sensor groups increased nonlinearly as the new load steps increased. No new hits were recorded at moments when no force was applied which is shown by plateaus.

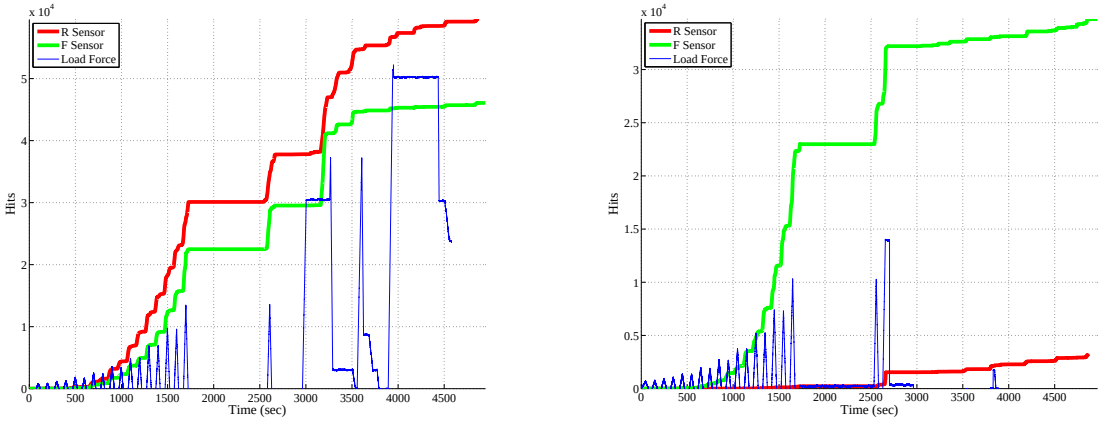

(a) North Side (b) South Side

Figure 4.12. Shear Wall One cumulative hits

More Hits were registered by the R sensor than the F sensor toward the end of the test. This finding indicates the R sensor was able to detect more signals that were not attenuated by damage. As expected, the F sensors for both the north and south sides of the wall were nearly identical in terms of the number of Hits as was expected. The R sensors did not record the same number of Hits. The total number for the R sensor was vastly greater for the north side of the wall which does not seem to follow the expected behavior for both of these sensor group layouts even though they were symmetrical.

The Hits are a good indicator of the damage as can be seen in the relationship between force and signals collected. More damage resulted in more signals recorded. It

can be seen in Figure 4.13 and those located in Appendices B7 that a higher number of Hits comes at the first of the two cycles, when new cracks were forming. After damage accumulated around 2700 seconds, more signals were recorded by the R sensors than the F sensors. This would be due to the attenuation of the higher frequencies by the cracked material. Sensors that were in areas of high damage recorded more Hits, the frequency analysis of these Hits show that as more force was applied, the average frequency centroid changes due to the effect of crack closing from compressive stresses. Frequency distributions can be seen for the sensor groups located at the different areas of interest in Appendix B8 thru B12. The trend of the average frequency centroid decreased for all of the R sensors, regardless of position when the amount of damage increased.

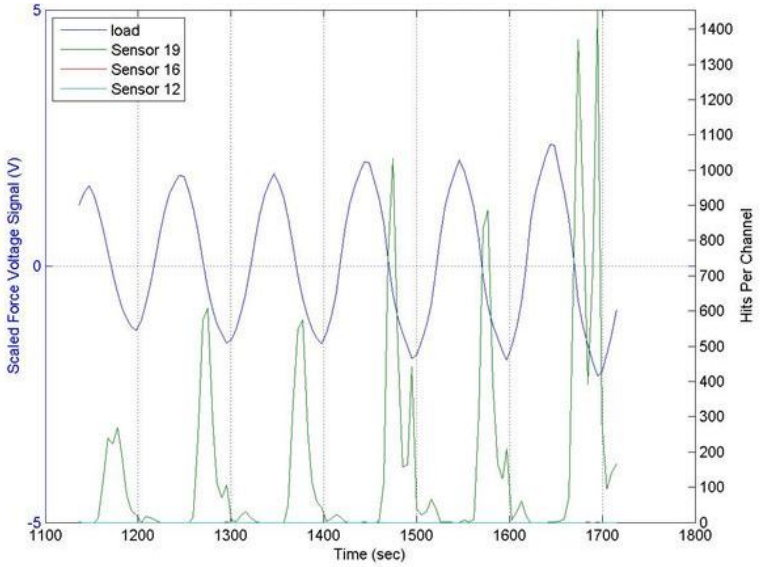

Figure 4.13. Shear wall one force and hits (channels 12,16 and 19 were located around the north (left) toe

The signal strength of the R sensor was examined in these tests because it is a good indicator of the type of waves being produced. The signal strength is the integral of the waveform representing energy being collected by the sensor. It is a relative value, since it is physically impossible to collect energy from cracking. The cumulated signal strength values (see Figure 4.14) increased for each individual hit after damage began to accumulate because the signals recorded were of a larger amplitude and longer length.

Many of AE signals that were collected (were continuous signals which have a significant higher number of counts) at points of significant cracking. The R sensor's signal strength was studied because larger values correspond significant damage. The sounds recorded for both correspond to brick spalling and significant crack growth.

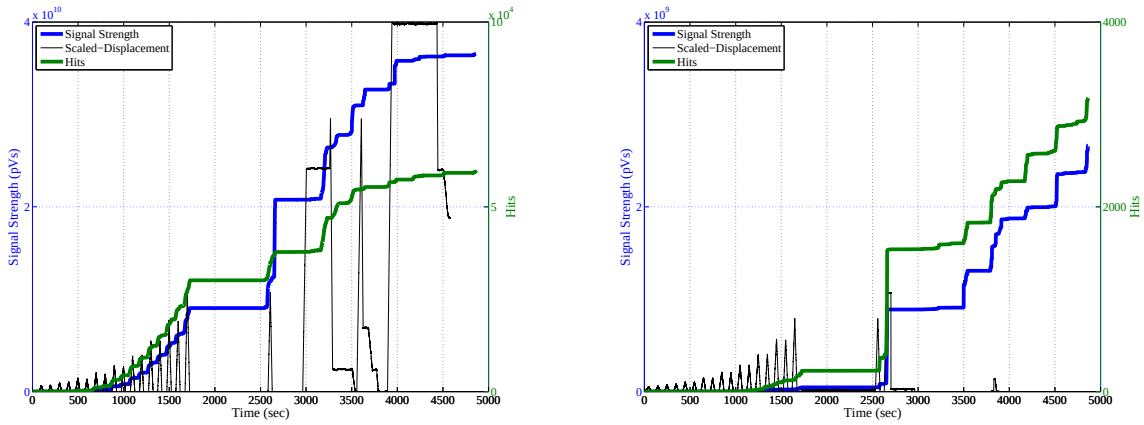

(a) North Side (b) South Side

Figure 4.14. Shear Wall One cumulative hits and signal strength

The amplitudes and counts for R sensors are shown in Figure 4.15. Each of these parameters increased as the cracking increased from the beginning of the test to its peak at 3500 seconds. Outliers in this analysis are mostly due to the collection of continuous waves or multiple waves within one recorded signal. These are a result of significant AE activity, which corresponded to the peak of each stroke. These plots represent the group of sensors within the designated group around each toe. Color has been added to these figures to help grasp time (in the depth axis of each plot). The R sensor on the north side recorded more hits than the south side. This observation has already been stated but another possible reason is the sensitivity of the sensor. It was determined that there was a defective sensor.

The R sensor was capable of detecting significant damage from over 5 feet away. In comparing the F and R sensor within the same zone, it can be seen that the increase in amplitude and counts occurred at the same time during the test. The higher number of counts of the F sensor would be due to the higher frequency. From analyzing these

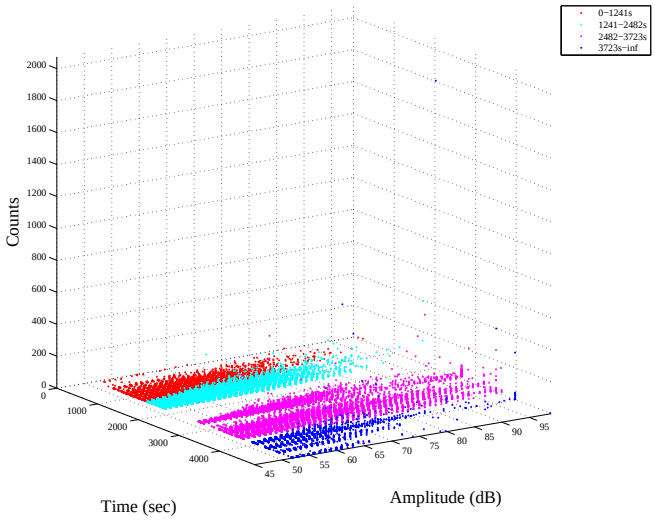

Figure 4.15. Shear Wall One R sensor counts and amplitude of individual hits

two plots, it should be clear that the higher number of lower frequency signals occurred as more of the material cracked and higher frequencies were attenuated.

The frequency content of recorded hits changed throughout the test as damage progressed. Figures 4.16 and 4.17 illustrate the average frequency centroid over time of test. These plots also include an average value and a standard deviation of this recorded data for each load cycle. It is difficult to determine a pattern of the standard deviation. The behavior of the average frequency content is random but it does represent a trend that as damage progressed, more frequencies are recorded in the lower range. Higher frequencies are attenuated. The F sensor captured a change in frequency, which correlates with the compressive force within this region.

The RA/AF component was studied in this analysis (Figure 4.18 and Appendices B3 and B4). The force's output has been included in these plots as a frame of reference for when damage occurred. Most of the values plotted are in the vertical axis, corresponding to tensile cracking. The type of sensor used did not affect the results that were gathered. The highest tensile signals came at moments of significant damage. It was believed that additional signals would be registered as shear cracks due to the particular damage;

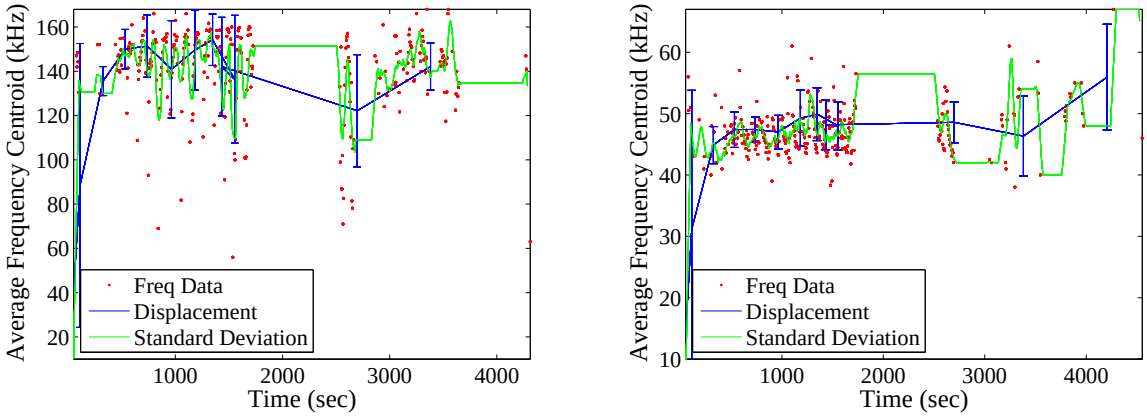

(a) North Side: Channel 13 (b) South Side: Channel 9

Figure 4.16. Sensor Wall One average frequency centroid F sensor at toe

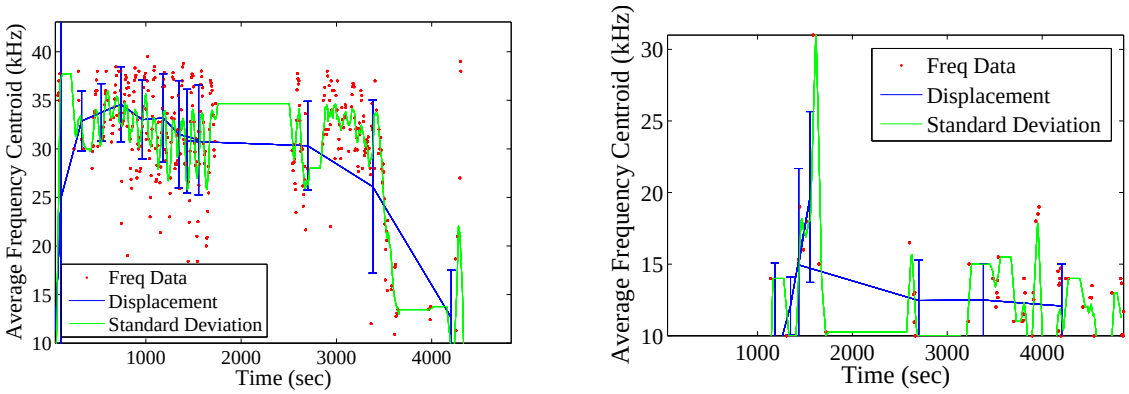

(a) North Side: Channel 14 (b) South Side: Channel 19

Figure 4.17. Sensor Wall One average frequency centroid R sensor at toe

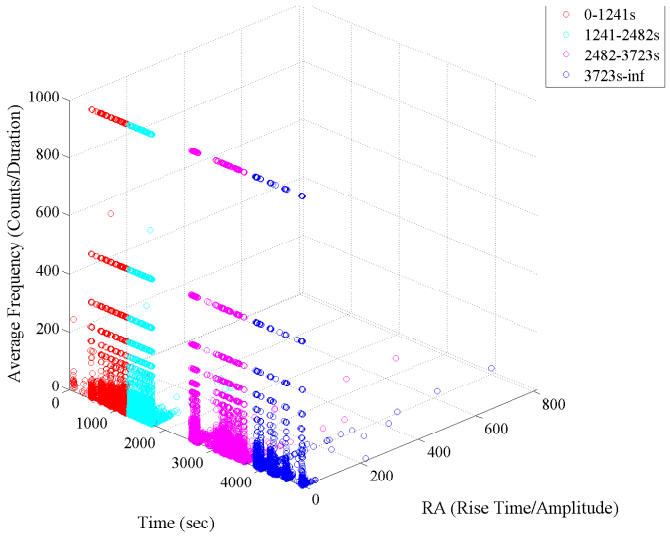

Figure 4.18. Shear Wall One RA/AF R sensor group on the north side

however, the diagonal shear crack that developed was not well represented in this analysis perhaps due to a loss of time synchronization.

4.5.2. Shear Wall Two. Both a new sensor arrangement and a new test setup, were expected to produce results that were different from those previously recorded. A large number of Hits in the second wall corresponded to significant damage. The actuator's scaled voltage output represents the wall's displacement. This analysis only includes the portion of the test taken from 0.25 inch to 2.75 inches displacement. The sensors data has been organized according to groups shown in Table 4.6.

Table 4.6. Shear Wall Two sensor group

Side	Type	Ch.	Ch.	Ch.	Ch.
North	F	4	5	2	
North	R	11	15	3	10
South	F	9	19	7	
South	R	17	20	16	21
Middle	R	12	24	14	

The R sensors collected a similar number of Hits even though the sensor layout was asymmetrical. The F and R sensors recorded more signals than Shear Wall One with 4 post-tension rods. Increases in the rate of Hits correspond with peaks of the displacement as can be seen in Figure 4.19. From looking at the R sensor curve, it can be seen that this group is including sensors that picked up damage from the other end of the wall. The increases in Hits between each displacement peak, which was unexpected, it was believed these signals would have been attenuated by the travel length.

Being able to detect signals over large periods does have promising attributes. The rate of collected signals captured by F sensors was nearly linear throughout this test for both the north and south sides of the wall. This trend can seen in the curve's overall slope. The sensor's slope was nonlinear. The rate which these sensors collected

Hits was higher than the F sensor when damage had occurred. This result is important because it indicates that damage has already occurred and is progressing to a higher degree. Additional signals were collected (as can be seen in these plots) as the cycle displacement step increased. The rate of signal strength for the R sensor again was larger than that of the Hits collected as damage accumulated. Values for signal strength were larger because the low frequency waves have a larger integral. This trend can be seen in Figure 4.20. Both the R Hits and signal strength are given in Appendix B25.

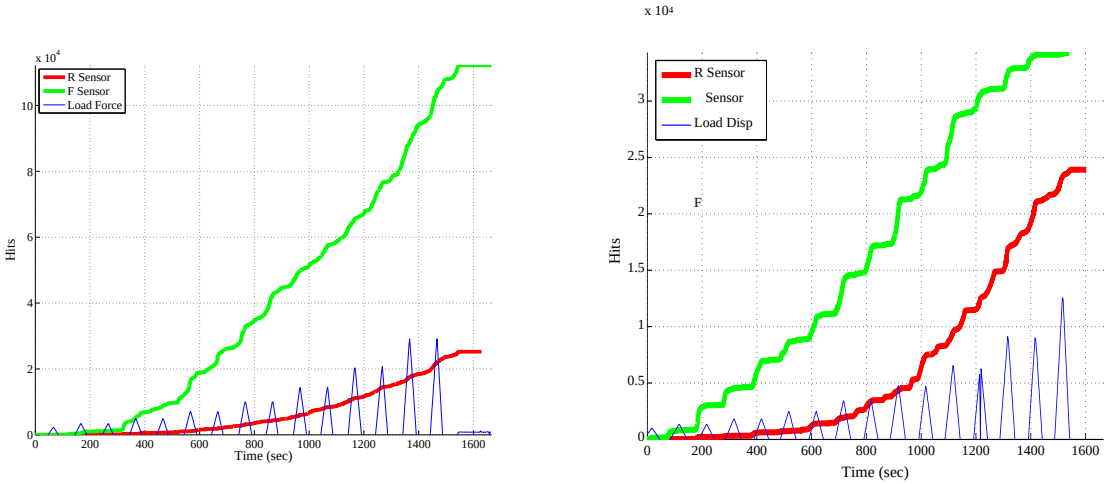

(a) North Side (b) South Side

Figure 4.19. Shear Wall Two cumulative hits

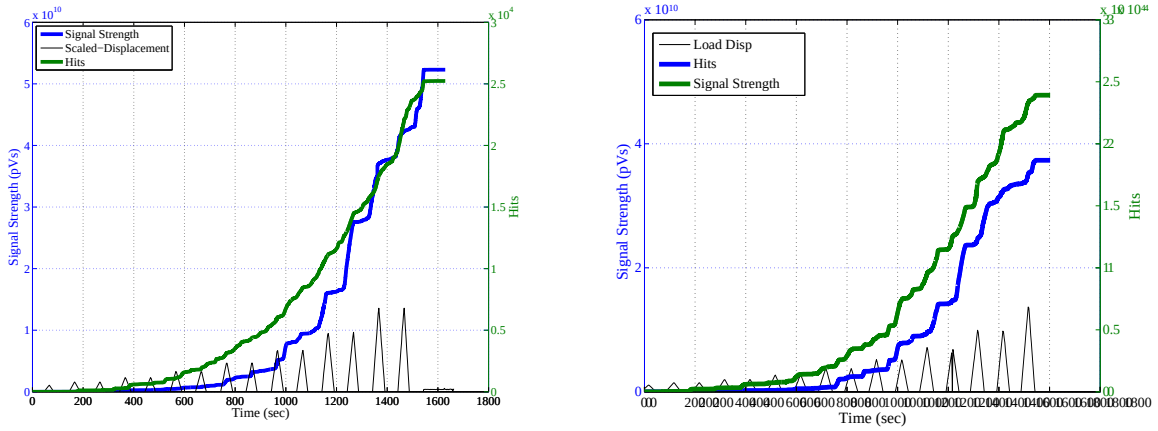

(a) North Side (b) South Side

Figure 4.20. Shear Wall Two cumulative signal strength and hits R Sensor

The F sensors successfully captured the change in displacement and the force on the wall. The centroid of the frequency decreased as the force was relieved. The microcracking events produced more signals that were bunched into a higher frequency domain. This finding is noted in F sensor channels 2 and 7 located in Figure 4.21. In looking at the F sensor at the north toe of the wall, the highest frequencies occurred before any visual indication of cracking existed. Sensor 10 became disconnected due to damage but still continued recording signals while resting on the foundation below and away from the cracking area (see Figure 4.22a).

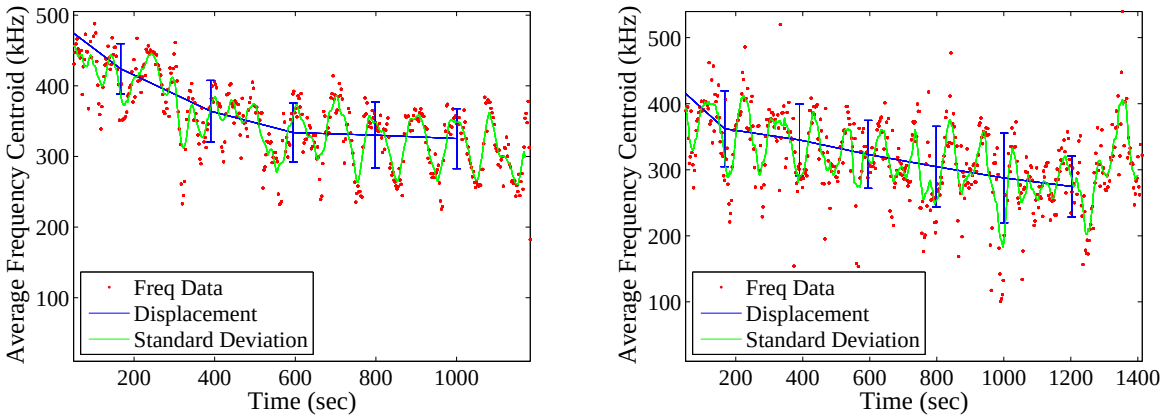

(a) North Side: Channel 2 (b) South Side: Channel 7

Figure 4.21. Sensor Wall Two average frequency centroid F sensor at toe

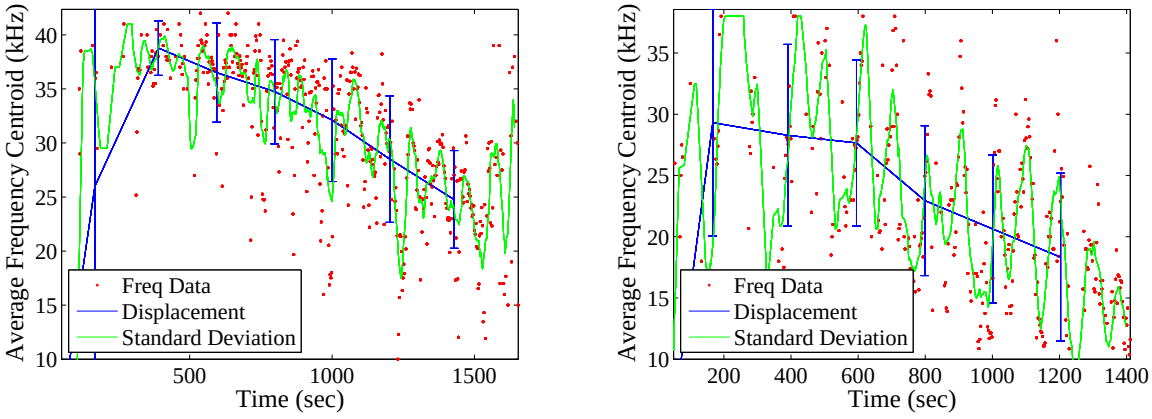

(a) North Side: Channel 10 (b) South Side: Channel 21

Figure 4.22. Sensor Wall Two average frequency centroid R sensor at toe

The signals collected by this sensor were of a similar response to the next closest R sensor. This highlights R1.5 sensor's sensitivity. The R sensor captured a higher number of lower frequency signals when additional damage occurred. This trend can be seen in the data from all R sensors located near the damaged areas.

The RA/AF had higher values in both axes. This is represents moments of significant crack growth. This can be seen in Figure 4.23 and Appendices B21 and B22 is universal for both sensor types. These plots shows a larger amount of signals in the horizontal axis, which is associated with shear cracks.

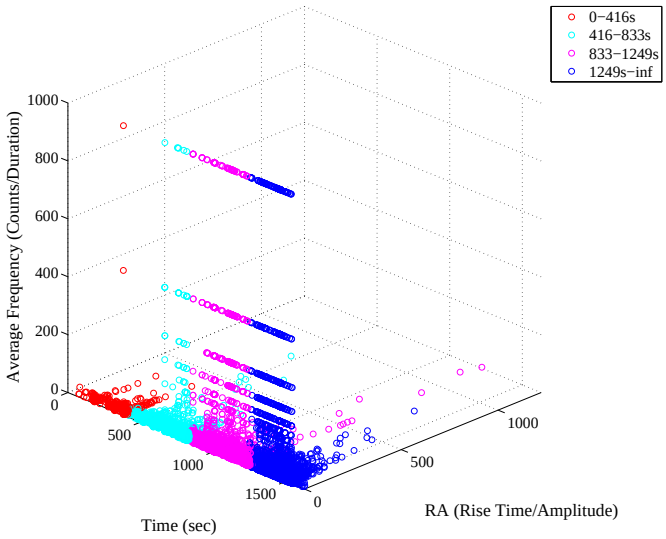

Figure 4.23. Shear Wall Two RA/AF R sensor group north side

It was expected that many shear cracking signals collected by sliding of Shear Wall Two against the foundation. This was not the case, many of the signals recorded by both the R and F sensor groups where in the tensile crack domain. These tensile cracks were lumped into particular values. This isn't physically possible and so poses the question of how the software determined average frequency.

4.6. CONCLUSION

Two walls were tested with two different post-tensioning configurations and two slightly different acoustic emission sensor layouts. These layouts included two different types of sensors that had vastly different peak resonant frequencies. The conclusion of this content is listed as similarities and differences between the two walls. This relates the results with sensor performance looking at trends that appeared in the data.

These similarities include the following:

- The damage that occurred was related to the release of Hits. High amplitudes, high counts were a direct result of damage. Signals created by significant cracking produced outliers in the count parameters.

- Microcracking preluded macrocracking. The microcracking was bunched into a higher frequency for both sensors. The cracking waves were registered ahead of visible signs of damage.

- At states of greater damage, there was an obvious increase in signal strength over Hits collected. This means that the Hits that were collected were mostly of a higher amplitude and larger wavelength. Signal strengths recorded by both sensor types were much higher at moments of significant damage. The R sensor, however was better at capturing the behavior of higher strength readings per recorded hit.

- The frequency centroid of signals decreased toward the latter portion of the test due to material damage. The damage resulted increased the sound attenuation. This was evident in the decrease of the frequency centroid of signals toward the latter portion of the test due to material damage. Cracks were also allowed to open during unloading further attenuating higher frequencies.

- The specimens' damage can be qualified by the difference in sensor performance between the two types. More signals were collected by the R sensor than were collected by the F sensor after damaged had accumulated due to the cracked material's attenuation.

Major differences between the two walls included the following:

- The second wall had less strength, stiffness and a higher total displacement. Further sliding was a result in the second wall. Greater energy dissipation is seen in the hysteresis of the second wall. Another issue of structural resistance is the decrease force after each complete cycle. The sliding produced a significant amount of signals which were registered by the R sensors at both ends of the wall. The time of test of second wall was shorter but the total number of recorded waves was much higher. In Shear Wall Two the different sensor layout recorded more signals over a larger area of the wall where damage might be occurring.

- One of the R sensor groups collected more Hits than the other side in Shear Wall One. The F sensor groups captured more signals than the other side in Shear Wall Two. Thus, several of the sensors used may lacked sensitivity. An analysis can still be made with comparative results based on how the cumulative curve is scaled.

- The actual values of the RA/AF values seem to be trivial. The second wall had more signals in the horizontal plane which corresponds to shear cracking, this would be indicative of more shearing sounds or a signal of long duration and small risetime coinciding with continuous waves. This could be caused by the sliding at the bed joint. This approach seems to provide information about structural behavior, though could not represent vertical or diagonal shear cracks when they did appear.

This approach captured the sounds of CMU as it was cracking. The sensor setup did not significantly impact the recorded results. As the wall damaged the sensors were able to identify changes to the material. Though useful for real time monitoring, in predicting the wall's ultimate strength, there are still many challenges. The approach taken was to

look at the overall data trend and determine how it related to wall's damage. Particular trends were identified in these tests. Additional tests using similar specimens could help verify these finds.

5. CONCLUSION

In these studies Acoustic Emission Technology was used to record sounds created by fracturing of bricks. Parameters of the signals were quantified and an analysis was made. This analysis looked at parameters such as amplitude, counts, signal strength, risetime, average frequency and frequency centroid. This approach incorporated two types of sensors, an R1.5 AST with a peak resonant frequency of 14 kHz and an F15i AST wideband AE sensor with a wide response in the 150 kHz range. The materials used in this study were made of concrete masonry units, grout, and mortar. This research focused on damage to a highly brittle, highly heterogeneous material using AE.

The tests were done on both small and large specimens. The first group of small specimens explored the behavior of adding rubber to CMU to improve ductility and resilience. AE sensors collected data throughout the test, observing damage and comparing results with force and displacement. The second study was a test of an entire structural wall system built to scale and incorporating an innovative post-tensioning system which promoted post yield strength. AE sensors were applied to the shear wall and damage was monitored. Results were compared between the different test setups.

As would be expected, damage due to cracking caused a release of elastic waves which were registered as individually recorded waves known as hits. A significant number of hits corresponded to damage; these coincided with the peak of each load step for all tests. For the purpose of obtaining good results, sensor hardware and software settings were adjusted to capture as little noise as possible. The threshold in these tests was increased and bandwidth adjusted to help eliminate noise.

This study compared the behavior of two sensor types used concurrently. Results were shown in R sensor groups and F sensor groups. Crack formation occurred at the start of a new load step. The load was applied with displacement control, a new load step was associated with a higher increment of displacement. At moments of significant cracking a release of sounds which were registered as hits. A higher number of hits

were associated with crack formation. These moments occurred toward the end of each step when the displacement was the highest, producing the highest stresses. Cumulated graphs of the recorded hits of each group were shown to represent the damage progression of the specimen. A steep slope of this curve would represent a significant collection of hits and this was correlated to peaks of each load step.

Another notable discovery was the relationship between frequency centroid and the material degradation. With a reduction in resistance due to cracking and at less stress, the frequency centroids tended to decrease. The R sensor was better at capturing this behavior with the given specimens. Signals collected by the F sensor were subjected to more attenuation and generally did not capture as many hits as the R sensor. The change in frequency centroid with the R sensor was an indicator of damage; it decreased with accumulated damage. Another observation can be seen in the general progression of amplitude and counts as the cracking became more severe. For all specimens, at higher stress higher amplitude counts levels were recorded. At the peaks of the stroke, continuous waves were recorded as a result of many sounds occurring at one given instance.

In examining the signal strength of the recorded signals, the signal strength which might keep on increasing as hit collection diminished. This behavior is representative of the integral of the larger and longer AE hits recorded during significant cracking at the end of the test. For specimens with a high percentage of rubber, attenuation reduced this effect. The higher signal strength would be due to larger waves with larger wavelengths, these would be collected during crack opening.

In addressing how this approach could be implemented on a real structural element, the sensing technology was applied to a full scale masonry shear wall which was tested cyclically until failure. In this study, post-tensioning had been incorporated into the shear wall design to allow for rocking movement. The sensors were used in two different layouts to capture the progression of damage to the entire shear wall. These layouts used two different sensor types to understand the phenomena of damage as the material cracked and spalled away from the grout core.

The benefit of the larger number of sensors was that comparisons could be made through differences in recorded spectrum. For starters, by studying the collection of hits, some initial conclusions could be made. The approach to this problem looked at parameters of the sensors output similar to the masonry prism tests but also considered the position of the sensors in gathering information. The anticipated location of damage was at the toes of the shear wall thus the F sensors were located in these regions to capture the start of microcracking. To help collect the results of these sensors, groups were formed and plots were produced from groups of sensors. The evolution of damage started from microcracking, leading to crack progression, followed by crack opening. After significant cracking, the brick spalled, and the grout crushed and finally a rapid shear crack propagated across the entire wall. Pictures were included to show the evolution of this failure mechanism and the final result of damage from the conclusion of the test. It was noticed that some of the results of the sensor groups were sporadic because of a lack of sensitivity of individual sensors.

From the AE analysis it was determined that the combination of two sensors was beneficial for detecting both microcracking and macrocracking leading to failure. This can be seen as a plateauing of the F sensor and an increase in the R sensor which was represented as nonlinear rate of R sensor hits collected. The R sensor was better at capturing the behavior of fracture through a decreased spectrum of the frequency centroids.

In general, the R sensors did not have to be placed within the vicinity of damage but were capable of detecting frequency changes at larger distances. Before it was visually apparent, F and R sensors that were located within the damaged zones were successful at capturing microcracking cracking. There was a correlation between the force applied to the wall and the frequency distribution. Just as in the prism tests, higher force let to higher recorded frequencies, which would be sensed more easily by the R sensor.

Cumulated values for hits, signal strength were shown in a number of combined plots for both tests. The results were grouped based on sensor type, location and data

parameter. Interestingly, at stages of higher damage fewer signals were recorded but those signals had a higher signal strength. The F sensor was less sensitive to damage at this stage because of the degradation of the material. The R sensor was more representative of the accumulation of signal strength. This clear behavior is useful in evaluating the state of the wall's damage when access to force or displacement information is inconvenient.

As speculated, tensile cracks would occur prior to shear cracks. The shear cracking sound would result from spalling of the brick and grinding of the wall against the foundation as it was physically moved during higher levels of displacement. In these experiments the RA/AF analysis was studied temporally to estimate the damage evolution. The RA/AF an indicator of tensile and shear cracking, didnt accurately demonstrate the contributions of shear cracking. The results of this approach represented most signals as tensile which isnt accurate. The RA/AF approach did relate moments of significant damage occurring at the peaks of load steps. The same approach, however, can be observed by looking at the amplitude of hits as shown in the peak amplitude-counts and time plots. The benefit of keeping track of these parameters is that there is a clear representation of the effect of damage over time.

By looking at the effects on these sensors over the time of the test, a lot of information can be gained about the fracturing of the material. Higher amplitudes and counts were associated with signals released at higher levels of load. These signals were generally registered as a higher frequency for the given sensors parameters. In observing increase of the rate of signal strength and rate of hits, when the rate of signal strength increased more than hits, damage was severe. When making a prediction about the strength of a specimen, it is evident that high amplitude, counts were the result of new crack growth and the reduction in frequency centroid corresponded to material degradation.

This approach to implementing this technology was for the purpose of simplifying a method of monitoring a large structure such as a CMU shear wall. This information is critical in the time of crisis and in helping protect the public from imminent or unforeseen

dangers. Though a significant amount of time was spent on the subject, there were concepts that could benefit from further exploration. Future work on this topic has been listed.

6. FUTURE WORK

There are potentially a few avenues worth traveling to tap into the behavior of AE sensors in capturing cracking sounds. A few suggestions came to mind after completing this work. Firstly, sounds collected from these tests were not just the brick cracking but also sounds from friction of bricks sliding. There may be an opportunity to isolate the sound of bricks sliding by performing some experiments while applying various levels of normal forces and inducing sliding.

In hindsight it would be advantageous to conduct more tests with the same experimental setup to have repeatably and higher degree of confidence. A comparison of known values from these sensor could provide more information on just the trends of this research but also quantitative cumulative values at the end of each test.

Attenuation was a big issue in these tests, performing a study on the attenuation with the material. Understanding the change of the amplitude and frequency of the source at varying distances would help for further comprehension. Possible attenuation tests could be performed testing the amplitude and frequency content of recorded signal by known sources over a variety of travel distances.

7. GLOSSARY

Acoustic Emission (AE): elastic waves generated by the rapid release of energy from sources within a material.

Aliasing: an effect that causes different signals to become indistinguishable when sampled. A distortion results from signals that are reconstructed from recorded waves sampled below the Nyquist frequency.

Amplitude: the voltage peaks in the AE signal waveform; which is generally expressed in decibels relative to 1 microvolt at the preamplifier input (dB).

Attenuation: loss of amplitude with distance as the wave travels through the test structure.

Average Frequency: the number counts divided by the duration of the entire signal

Average Signal Strength: the average of signal strength values of the hits recorded over a given time period.

Bandpass Filter: a device that passes frequencies within a certain range, omitting frequencies that are outside of that range.

Burst Emission: a qualitative description of the discrete signal related to an individual emission event occurring within the material.

Calm Ratio: AE activity during unloading/AE activity during previous maximum loading.

Channel: a single AE sensor and its related equipment components for transmitting, conditioning, detecting and measuring signals.

Continuous Emission: a qualitative description of the sustained signal level produced by rapidly occurring acoustic emission events.

Counts to Peak: number of times when a waveform passes the threshold level before reaching a maximum amplitude.

Counts: the number of times when the AE signal crosses the detection threshold. Also known as ringdown counts and threshold crossing counts.

Cumulative Signal Strength: the addition of the signal strength of each hit over time.

Detection: recognition of the presence of a signal (typically accomplished by the signal crossing a detection threshold.

Duration: the time from the beginning of first threshold crossing to the last threshold crossing by the recorded signal.

Energy: the parameter derived from the integral of the rectified voltage signal over the entire duration of the AE hit.

Event Definition Time: the time allowed for recording waveforms (hits) in a sensor group from a given signal.

Event Lockout Time: the time interval in between two events.

Event: a local material change giving rise to acoustic emission.

Fast Fourier Transform: an algorithm to compute the discrete Fourier transform representing a waveform with in the frequency spectrum.

Felicity Effect: Upon reloading significant amount of signals collected prior to arriving to a previous maximum load.

Felicity Ratio: defined as load ratio at onset of significant AE activity in the current load cycle to maximum load in the previous loading history.

Frequency Centroid: a measurement within signal processing to characterize a spectrum. It indicates the center of mass of the spectrum. Posted as equation 3.1.

Frequency Spectrum: A representation of a recorded waveform in the frequency domain.

Frequency: for an oscillating signal or process, the number of cycles occurring in unit time.

Guard Sensors: sensors whose primary function is the elimination of extraneous noise based on arrival time differences.

High Pass Filter: a filter that passes signals with a frequency higher than a certain cutoff frequency.

Hit Definition Time: the time constant used to terminate the measurement of a signal.

Hit Lockout Time: the period of time after a hit in which no new hits will be recorded.

Hit: the process of detecting and measuring an AE signal on a channel.

Kaiser Effect: load levels that have been previously exerted on a material do not produce AE activity. This phenomenon is material specific.

Load Ratio: the measure of AE activity consistently decreased with increasing loadsets (increasing levels of damage). This measure is more useful than others for assessing post-yield damage.

Low Pass Filter: a filter that passes signals with a frequency lower than a certain cutoff frequency.

Max Duration: sets the length of the recorded wave. The max duration function is important when the signal is staying above the threshold more-or-less continuously due to noise or extremely high AE activity.

Noise: any undesirable signal detected by sensors.

Nyquist Frequency: a cutoff frequency that allows for a perfect reconstruction of a signal.

Parametric Inputs: an input voltage representing a measured quantity such as temperature, pressure or strain.

Peak Amplitude: the highest amplitude of the waveform.

Peak Definition Time: the time parameter that allows to define a particular peak in terms risetime and amplitude.

Preamplifier: a built-in amplifier within the sensor which amplifies the signal before it is transmitted to the receiver.

Rectifier: an electrical device that converts an alternating current, which periodically reverses direction, to direct current.

Relaxation Ratio: this measure provides similar results to the calm ratio for the flexural specimens.

Resonant Frequency: a frequency which causes the highest amplification of a system response.

Risetime: the time it takes a waveform to achieve a peak value from the first threshold crossing.

Sampling Rate: a discrete number of samples per second taken from a continuous signal.

Sensor Group: designated sensors which record signals from the same source.

Sensor: a device containing a transducing element that turns AE wave motion into an electrical voltage.

Short Time Fourier Transform: a Fourier-related transform of a small segment of a signal used to determine the frequency and phase content of local sections of a signal as it changes over time.

Signal Strength: the measured area of the rectified AE signal with units proportional to volt-seconds. Signal: a function or sequence coming from the transducing element and passing through subsequent signal conditioning equipment (amplifiers, frequency filters).

Source: the physical origin of one or more AE events.

Threshold: a predetermined energy level which triggers the recording of a signal.

Time of Hit: the time in which the beginning of the signal detected or the first crossing of the threshold by the recorded wave.

APPENDIX

GRAPHICAL DATA FROM EXPERIMENTS WITH MASONRY PRISMS AND MASONRY SHEAR WALLS

INTRODUCTION

Included with this Thesis is a CD-ROM, which contains more graphical data and images from this research. The data is divided into two sections covering both sets of experiments. The file is saved as a PDF.

BIBLIOGRAPHY

1. Carpinteri, A., A. Grazzini, G. Lacidogna and A. Manuello (2014). "Durability evaluation of reinforced masonry by fatigue tests and acoustic emission technique". Structural Control and Health Monitoring 21(6): 950-961.

2. Carpinteri, A. and G. Lacidogna (2007). "Damage evaluation of three masonry towers by acoustic emission". Engineering structures 29(7): 1569-1579.

3. Carpinteri, A., G. Lacidogna and G. Niccolini (2007). "Acoustic emission monitoring of medieval towers considered as sensitive earthquake receptors". Natural Hazards and Earth System Science 7(2): 251-261.

4. Carpinteri, A., G. Lacidogna and G. Niccolini (2011). "Damage analysis of reinforced concrete buildings by the acoustic emission technique". Structural Control and Health Monitoring 18(6): 660-673.

5. Cartz, L. (1995). "Nondestructive testing. ASM International". The Materials Information Society, Materials Park, OH.

6. Castellanos, F. and M. Ordaz (2014). "Damage severity estimation of an elastoplastic singledegreeoffreedom oscillator from its ground and response accelerations". Structural Control and Health Monitoring 21(1): 1-22.

7. Colombo, S., M. Forde, I. Main and M. Shigeishi (2005). "Predicting the ultimate bending capacity of concrete beams from the 'relaxation ratio' analysis of AE signals". Construction and Building Materials 19(10): 746-754.

8. Dawson, B. (1976). "Vibration condition monitoring techniques for rotating machinery". The shock and vibration digest 8: 12. Elgawady, M. and A. Gheni (2014). Strength of Unbonded Post-Tensioned Walls.

9. Enoki, M., T. Kishi and S. Kohara (1986). "Determination of Micro-cracking Moment Tensor of Quasi-cleavage Facet by AE Source Characterization". Progress in Acoustic Emission III, JSNDI: 763-770.

10. Farhidzadeh, A., E. Dehghan-Niri, S. Salamone, B. Luna and A. Whittaker (2012). "Monitoring crack propagation in reinforced concrete shear walls by acoustic emission". Journal of Structural Engineering 139(12).

11. Farhidzadeh, A., A. C. Mpalaskas, T. E. Matikas, H. Farhidzadeh and D. G. Aggelis (2014). "Fracture mode identification in cementitious materials using supervised pattern recognition of acoustic emission features". Construction and Building Materials 67: 129-138.

12. Farhidzadeh, A. and S. Salamone (2012). Introducing sifted b-value analysis and a new crack classification for monitoring reinforced concrete shear walls by acoustic emission. 54 th Acoustic Emission Working Group Meeting, Princeton, NJ, USA (Student paper award).

13. Farhidzadeh, A., S. Salamone and P. Singla (2013). "A probabilistic approach for damage identification and crack mode classification in reinforced concrete structures". Journal of Intelligent Material Systems and Structures 24(14): 1722-1735.

14. Golaski, L., P. Gebski and K. Ono (2002). "Diagnostics of reinforced concrete bridges by acoustic emission". Journal of acoustic emission 20(2002): 83-89.

15. Holford, K. and R. Lark (2005). "Acoustic Emission Testing Bridges".

16. Hu, S., J. Lu and F. Xiao (2013). "Evaluation of concrete fracture procedure based on acoustic emission parameters". Construction and Building Materials 47: 1249-1256.

17. Hutton, P. and J. Skorpik (1977). Acoustic Emission Methods for Flaw Detection in Steel Highway Bridges, Report No. DOT-FH-11-904, FHWA R&D 78-97, Battelle Northwest Laboratory, Richland, Wash.

18. Kaphle, M., A. C. Tan, D. P. Thambiratnam and T. H. Chan (2012). "Identification of acoustic emission wave modes for accurate source location in platelike structures". Structural control and health monitoring 19(2): 187-198.

19. Kishi, T. (1999). "A proposed standard for evaluating structural integrity of reinforced concrete beams by acoustic emission". Acoustic emission: standards and technology update 25.

20. Knill, J., J. Franklin and A. Malone (1968). A study of acoustic emission from stressed rock. International Journal of Rock Mechanics and Mining Sciences & Geomechanics Abstracts, Elsevier.

21. Liu, Z. and P. H. Ziehl (2009). "Evaluation of reinforced concrete beam specimens with acoustic emission and cyclic load test methods". ACI Structural Journal 106(3).

22. Losert, R. (2009). "Solution for NDT inspection". NDT Magazine.

23. Matsuyama, K. and M. Ohtsu (1992). "Rate process analysis of AE activity to evaluate the deterioration of concrete by core tests". Proceeding of the AECM-4, ASNT 132(8).

24. Muhamad Bunnori, N., R. Pullin, K. M. Holford and R. Lark (2006). "A practical investigation into acoustic wave propagation in concrete structures". Advanced Materials Research 13: 205-212.

25. Muravin, B. (2009). "Acoustic emission science and technology". Journal of Building and Infrastructure Engineering of the Israeli Association of Engineers and Architects.

26. Ohtsu, M. (1989). "Diagnostics of cracks in concrete based on acoustic emission". ACI Special Publication 112.

27. Ohtsu, M., T. Okamoto and S. Yuyama (1998). "Moment tensor analysis of acoustic emission for cracking mechanisms in concrete". ACI Structural Journal 95(2).

28. Ohtsu, M., M. Uchida, T. Okamoto and S. Yuyama (2002). "Damage assessment of reinforced concrete beams qualified by acoustic emission". ACI Structural Journal 99(4).

29. Ohtsu, M. and H. Watanabe (2001). "Quantitative damage estimation of concrete by acoustic emission". Construction and Building Materials 15(5): 217-224.

30. Ohtsu, M. and S. Yuyama (2000). Recommended practice for in situ monitoring of concrete structures by acoustic emission. 15 th International Acoustic Emission Symposium.

31. Ouyang, C., E. Landis and S. P. Shah (1991). "Damage assessment in concrete using quantitative acoustic emission". Journal of Engineering Mechanics 117(11): 2681-2698.

32. Parmar, D. and S. Sharp (2009). Acoustic emission for non-destructive testing of bridges and other transportation infrastructure. Beyond the crossroads: A national conference on transportation infrastructure & regulatory policy, Denver, CO.

33. Paulson, P., J. Elliott and D. Youdan (2001). "Continuous acoustic monitoring of bridges (Akustisches berwachungssystem fr Brcken". Stahlbau 70(4): 245-250.

34. Prosser, W., M. Hamstad, J. Gary and A. O'Gallagher (1999). "Finite element and plate theory modeling of acoustic emission waveforms". Journal of nondestructive evaluation 18(3): 83-90.

35. Shamina, O. (1956). "Elastic pulses in the fracture of specimens of rocks". Izv. Akad. Nauk SSSR, Ser. Geofizicheskaya(5): 513-518.

36. Shokouhi, P., A. Zoga, H. Wiggenhauser and G. Fischer (2012). "Surface wave velocity-stress relationship in uniaxially loaded concrete". ACI Materials Journal 109(2).

37. Uddin, F. A., M. Shigeishi and M. Ohtsu (2006). "Fracture mechanics of corrosion cracking in concrete by acoustic emission". Meccanica 41(4): 425-442.

38. Vinogradov, S. (1964). Acoustic Observations of the Processes of Fracture of Rocks, Nauka, Moscow.

39. Wu, C., G. Chen, J. S. Volz, R. K. Brow and M. L. Koenigstein (2012). "Local bond strength of vitreous enamel coated rebar to concrete". Construction and Building Materials 35: 428-439.

40. Yuyama, S. (2005). "Acoustic emission for fracture studies using moment tensor analysis". Journal of Strain Analysis for Engineering Design 40(1): 33-44.

VITA

John Alexander Cain, known personally as Alex Cain, was born in Milwaukee, Wisconsin. He graduated from Wauwatosa East High School and attended The University of Wisconsin-Milwaukee and Missouri University of Science and Technology for completion of his Master's Degree in Civil Engineering in December 2015.

His interests being in both engineering and music, he achieved a Bachelors of Science and Bachelors in Fine Arts while attending UWM. He was able to accomplish both the BS and BFA degrees sequentially, with some time off in between. Before reentering University, he was employed as a private music teacher, musician and owner of a small professional painting service.

While studying Civil Engineering at UWM as an undergraduate researcher, he researched in the area concrete technology, working with Dr. Konstantin Sobolev and Dr. Jian Zhao. As a student, he had interned at Milwaukee Metropolitan Sewerage District and Joehnk Engineering Group. Also at UWM, he was involved in student organizations. He captained the ASCE concrete canoe and was involved with The National Society of Black Engineers.

While at Missouri University of Science and Technology, he has researched in area of structural health monitoring using AE, fiber optics strain sensors and Smart Rock bridge scour monitoring.